doi: 10.17951/a.2019.73.2.135-173

ANNALES
UNIVERSITATIS MARIAE CURIE-SKŁODOWSKA
LUBLIN – POLONIA

VOL. LXXIII, NO. 2, 2019 SECTIO A 135–173

MASSIMILIANO D. ROSINI

Systems of conservation laws with discontinuous fluxes and applications to traffic

Dedicated to Yuri Kozitsky on the occasion of his 70th birthday

Abstract. In this paper we study 2×2 systems of conservation laws with discontinuous fluxes arising in vehicular traffic modeling. The main goal is to introduce an appropriate notion of solution. To this aim we consider physically reasonable microscopic follow-the-leader models. Macroscopic Riemann solvers are then obtained as many particle limits. This approach leads us to develop six models. We propose a unified way to describe such models, which highlights their common property of maximizing the density flow across the interface under *appropriate* physical restrictions depending on the case at hand.

1. Introduction

In this paper we consider the 2×2 system of partial differential equations

$$\begin{cases} \rho_t + \mathsf{f}(\rho, w, x)_x = 0, & t > 0,\ x \in \mathbb{R}, \\ w_t + \mathsf{v}(\rho, w, x)\, w_x = 0, & t > 0,\ x \in \mathbb{R}, \end{cases} \tag{1.1}$$

2010 *Mathematics Subject Classification.* 35R05, 35L65, 35L45, 90B20, 34A34.

Key words and phrases. Conservation laws, Aw–Rascle–Zhang model for vehicular traffic, discontinuous flux, follow-the-leader model, Riemann solvers, point constraint on the flux, point constraint on the velocity.

where (ρ, w) is the unknown variable, v is a possibly discontinuous function of x and

$$\mathsf{f}(\rho, w, x) \doteq \rho\, \mathsf{v}(\rho, w, x). \tag{1.2}$$

More precisely, $u \doteq (\rho, w)$ takes values in

$$\Omega \doteq \big\{(\rho, w) \in [0, +\infty)^2 : w > 0,\ w \geq p(\rho)\big\},$$

with $p\colon [0, +\infty) \to [0, +\infty)$ satisfying

(**A.1**) $p \in \mathbf{C^2}((0, +\infty); \mathbb{R})$, $p'(\rho) > 0$, $2p'(\rho) + \rho\, p''(\rho) > 0$ for every $\rho > 0$.

A possible choice is $p(\rho) \doteq \rho^\gamma$, $\gamma > 0$. Furthermore, $\mathsf{v}\colon \Omega \times \mathbb{R} \to [0, +\infty)$ has the form

$$\mathsf{v}(u, x) \doteq \mathsf{v}_-(u) \cdot \mathbb{1}_{\mathfrak{R}_-}(x) + \mathsf{v}_+(u) \cdot \mathbb{1}_{\mathfrak{R}_+}(x), \tag{1.3}$$

with

$$\mathfrak{R}_- \doteq (-\infty, 0), \qquad \mathfrak{R}_+ \doteq [0, +\infty),$$

and for some functions $\mathsf{v}_\pm\colon \Omega \to [0, +\infty)$ that are weakly decreasing and chosen according to the case under consideration. Above and after $\mathbb{1}_A$ is the indicator function of set $A \subset \mathbb{R}$. By (1.2), (1.3) we have that $\mathsf{f}\colon \Omega \times \mathbb{R} \to [0, +\infty)$ has the form

$$\mathsf{f}(u, x) \doteq \mathsf{f}_-(u) \cdot \mathbb{1}_{\mathfrak{R}_-}(x) + \mathsf{f}_+(u) \cdot \mathbb{1}_{\mathfrak{R}_+}(x), \tag{1.4}$$

with $\mathsf{f}_\pm(\rho, w) \doteq \rho\, \mathsf{v}_\pm(\rho, w)$. We assume that

(**A.2**) for any $w > 0$ the map

$$\mathsf{f}(\cdot, w)\colon [0, p^{-1}(w)] \to [0, +\infty)$$

is Lipschitz continuous, piecewice regular and concave.

System (1.1) can be interpreted as a generalization of the Aw, Rascle, Zhang (ARZ) model [13, 36] for vehicular traffic to the case of a non-homogeneous road. For this reason below we refer to $t > 0$ as time, $x \in \mathbb{R}$ as space, $\mathfrak{R}_-$ as incoming road, $\mathfrak{R}_+$ as outgoing road, $x = 0$ as junction, ρ as density, v as velocity, f as density flux and w as Lagrangian marker. In particular in Sections 4, 5 and 6 we consider two roads characterized by different capacities (i.e., maximal flows) or by different speed limits, or both.

The first equation in (1.1) is a conservation law and expresses the conservation of the total number of vehicles. The second equation in (1.1) is a transport equation and formally implies that w is transported at the velocity v of the vehicles. Away from the vacuum, system (1.1) is equivalent to the 2×2 system of conservation law

$$\begin{cases} \rho_t + \mathsf{f}(\rho, w, x)_x = 0, & t > 0,\ x \in \mathbb{R}, \\ (\rho\, w)_t + \big(\mathsf{v}(\rho, w, x)\, \rho\, w\big)_x = 0, & t > 0,\ x \in \mathbb{R}. \end{cases}$$

To the best of author's knowledge, there is no literature on 2×2 systems of conservation laws with discontinuous fluxes. We refer the reader interested in the scalar case to [1–8, 10–12, 14–17, 20–27, 30, 32–35].

The derivatives in (1.1) are interpreted in the sense of distributions. In fact, even for smooth density flux f and smooth initial data, classical solutions may not exist globally in time since discontinuities can arise in finite time. It is therefore necessary to consider weak solutions. Yet weak solutions are in general not unique. This motivates in [9] the introduction of entropy conditions *à la* Kruzhkov [28], which select a unique weak solution, at least away from the vacuum $\rho = 0$ and under the assumption that the road is homogeneous, namely $\mathsf{f}_- \equiv \mathsf{f}_+$.

Our main concern is to introduce an appropriate notion of solution for (1.1) to *uniquely* select a physically reasonable weak solution to a Cauchy problem. This can be achieved by choosing a unique Riemann solver

$$\mathcal{RS}_{\mathfrak{R}_-,\mathfrak{R}_+} : \Omega^2 \to \mathbf{BV}(\mathbb{R}; \Omega),$$

which by definition associates to any pair $(u_L, u_R) \in \Omega^2$ with

$$u_L \doteq (\rho_L, w_L), \qquad u_R \doteq (\rho_R, w_R),$$

a unique self-similar weak solution $u(t,x) \doteq \mathcal{RS}_{\mathfrak{R}_-,\mathfrak{R}_+}[u_L, u_R](x/t)$ to the Cauchy problem for (1.1) with Riemann initial condition

$$u(0,x) = u_L \cdot \mathbb{1}_{\mathfrak{R}_-}(x) + u_R \cdot \mathbb{1}_{\mathfrak{R}_+}(x), \quad x \in \mathbb{R}. \tag{1.5}$$

In fact choosing a Riemann solver corresponds to select the admissible discontinuities. The key point is to select the admissible discontinuities along the interface $x = 0$ and those involving a vacuum state $u = (\rho, w) = (0, w)$, $w > 0$. Indeed, the entropy conditions introduced in [9] do not take into account for the presence of the interface and do not uniquely select a solution when a vacuum state is involved. We make this point apparent in the following Definition 1.1. We denote by

$$\mathcal{RS} : \Omega^2 \to \mathbf{BV}(\mathbb{R}; \Omega)$$

the Riemann solver introduced in [13, 36] for ARZ model; we defer its definition to Section 2.

Definition 1.1. Fix a Riemann solver $\mathcal{RS}_{\mathfrak{R}_-,\mathfrak{R}_+} : \Omega^2 \to \mathbf{BV}(\mathbb{R}; \Omega)$. Let $\bar{u}$ be in $\mathbf{L^\infty}(\mathbb{R}; \Omega)$. We say that $u \in \mathbf{C^0}\big([0, +\infty); \mathbf{L^1_{loc}}(\mathbb{R}; \Omega)\big)$ is a solution to the Cauchy problem for (1.1) with initial condition

$$u(0,x) = \bar{u}(x), \qquad x \in \mathbb{R}, \tag{1.6}$$

if the following conditions are satisfied:

(1) u is a weak solution to (1.1), (1.6).

(2) u satisfies the entropy conditions given in [9] in both $(0, +\infty) \times (-\infty, 0)$ and $(0, +\infty) \times (0, +\infty)$.

(3) If u has discontinuities along the curve $x = \sigma(t)$, then its traces $u(t, \sigma(t)^-)$ and $u(t, \sigma(t)^+)$ satisfy the following conditions:

(a) for a.e. $t > 0$, if the discontinuity $x = \sigma(t)$ occurs away from $x = 0$ and involves a vacuum state, then

$$\mathcal{RS}[u(t, \sigma(t)^-), u(t, \sigma(t)^+)](\nu) = \begin{cases} u(t, \sigma(t)^-) & \text{if } \nu < 0, \\ u(t, \sigma(t)^+) & \text{if } \nu \geq 0, \end{cases}$$

(b) for a.e. $t > 0$, if the discontinuity $x = \sigma(t)$ occurs at $x = 0$, then

$$\mathcal{RS}_{\mathfrak{R}_-, \mathfrak{R}_+}[u(t, 0^-), u(t, 0^+)](\nu) = \begin{cases} u(t, 0^-) & \text{if } \nu < 0, \\ u(t, 0^+) & \text{if } \nu \geq 0. \end{cases}$$

Some comments on the above definition are in order. Condition **(2)** deals with discontinuity away from the interface $x = 0$. The discontinuities along $x = 0$ are considered in **(3)**, **(b)**. Furthermore, the entropy conditions introduced in [9] and used in **(2)** do not select a unique solution if a vacuum state is involved. This motivates condition **(3)**, **(a)**.

Our choice for the macroscopic Riemann solver $\mathcal{RS}_{\mathfrak{R}_-, \mathfrak{R}_+}$ stems from a microscopic follow-the-leader (FTL) model. The main advantage of this approach is that it requires to set assumptions on the interacting behavior of the vehicles only at the microscopic level. Since traffic dynamics are essentially microscopic, it is easier to physically motivate microscopic rather than macroscopic assumptions. We thus first adapt to (1.1) the (scalar) microscopic FTL approximation proposed in [19] for the (2×2 system) ARZ model. We then rely on a passage to the limit similar to that performed in [19]. At last we obtain $\mathcal{RS}_{\mathfrak{R}_-, \mathfrak{R}_+}$ as many particle limit by applying, at the level of numerical simulations and for carefully identified sets of data, an approximation procedure adapted from [19].

It turns out that at the limit we get the Riemann solver which maximizes the flow at $x = 0$ under some *appropriate* physical restrictions depending on the case under consideration. Let us underline that we do not require (explicitly) any maximization property at the microscopic level, as we only prescribe elementary vehicle interaction rules.

At last, we consider the case of pointwise bottlenecks, and show how a zooming process allows to build a model for point constraint on the flow or on the velocity, starting from those previously introduced.

This paper is organized as follows. For completeness, in Section 2 we recall the ARZ model [13, 36] for the homogeneous case. In Section 3, we give in Definition 3.1 a general definition of the Riemann solver for Riemann problem (1.1), (1.5) and motivate its introduction via a general FTL model (3.2). In Sections 4, 5, and 6, we consider specific cases with the two sections of the road characterized by different maximal flows, maximal speeds and by both maximal flows and speeds, respectively. For each of these cases we propose two approaches. At last in Section 7, we propose two approaches

to derive from the previous results traffic models with point constraints on the flow or on the velocity.

2. Riemann solver $\mathcal{RS}$ for ARZ model

In this section we recall the ARZ model [13,36] for vehicular traffic along a homogeneous road. It is expressed by the 2×2 system of partial differential equations

$$\begin{cases} \rho_t + (\rho\, v)_x = 0, & t > 0,\ x \in \mathbb{R}, \\ w_t + v\, w_x = 0, & t > 0,\ x \in \mathbb{R}. \end{cases} \tag{2.1}$$

Here $\rho = \rho(t,x) \geq 0$ and $v = v(t,x) \geq 0$ are the traffic density and velocity at time $t \geq 0$ and position $x \in \mathbb{R}$ along a one-lane homogeneous road. Moreover, $w > 0$ is a Lagrangian marker characterizing lengths and maximal speeds of the vehicles. The link between these quantities is expressed by the state equation

$$v = w - p(\rho), \tag{2.2}$$

where $p\colon [0,+\infty) \to [0,+\infty)$ satisfies (**A.1**), is an anticipation factor and takes into account drivers reactions to the state of traffic in front of them. The first equation in (2.1) expresses the conservation of the total number of vehicles, while the second equation in (2.1) is a transport equation and formally implies that w is transported at the velocity v of the vehicles.

A general notion of solution which enables to uniquely select a physically reasonable weak solution to Cauchy problems for (2.1) can be based on the definition of the Riemann solver $\mathcal{RS}\colon \Omega^2 \to \mathbf{BV}(\mathbb{R};\Omega)$ introduced in [13,36] by applying Definition 1.1. We stress that the entropy conditions *à la* Kruzhkov [28] introduced in [9] select a unique weak solution only away from the vacuum $\rho = 0$. Moreover, in [19] the authors rigorously deduced the ARZ model from a microscopic FTL model as many particle limit, but did not prove the uniqueness of the limit.

We conclude this section by recalling the definition of the Riemann solver $\mathcal{RS}\colon \Omega^2 \to \mathbf{BV}(\mathbb{R};\Omega)$ for the ARZ model (2.1), (2.2). We first need to introduce some notation. Let $v,\ f\colon \Omega \to [0,+\infty)$ be defined by

$$v(u) \doteq w - p(\rho), \qquad f(u) \doteq \rho\, v(u). \tag{2.3}$$

For any $w > 0$, let

$$\lambda_w\colon [0, p^{-1}(w)] \to [-p^{-1}(w)\, p'(p^{-1}(w)), w]$$

be defined by $\lambda_w(\rho) \doteq w - p(\rho) - \rho\, p'(\rho)$ and let

$$\mathcal{R}_w\colon [-p^{-1}(w)\, p'\big(p^{-1}(w)\big), w] \to [0, p^{-1}(w)]$$

be its inverse function. Notice that $\partial_\rho f(\rho, w) = \lambda_w(\rho)$. Let $s\colon \{(u_L, u_R) \in \Omega \times \Omega : \rho_L \neq \rho_R\} \to \mathbb{R}$ be defined by

$$s(u_L, u_R) \doteq \frac{f(u_R) - f(u_L)}{\rho_R - \rho_L}.$$

Define

$$[a]_+ \doteq \max\{a, 0\}.$$

Definition 2.1. The Riemann solver $\mathcal{RS}\colon \Omega^2 \to \mathbf{BV}(\mathbb{R}; \Omega)$ for the ARZ model (2.1), (2.2) is defined as follows:

(L.1) If $u_L, u_R \in \Omega$ with $w_L \neq w_R$ and $v(u_L) = v(u_R)$, then

$$\mathcal{RS}[u_L, u_R](\nu) \doteq \begin{cases} u_L & \text{if } \nu < v(u_{L,R}), \\ u_R & \text{if } \nu \geq v(u_{L,R}). \end{cases}$$

(L.2) If $u_L, u_R \in \Omega$ with $w_L = w_R$ and $v(u_R) < v(u_L)$, then

$$\mathcal{RS}[u_L, u_R](\nu) \doteq \begin{cases} u_L & \text{if } \nu < s(u_L, u_R), \\ u_R & \text{if } \nu \geq s(u_L, u_R). \end{cases}$$

(L.3) If $u_L, u_R \in \Omega$ with $w_L = w_R$ and $v(u_L) < v(u_R)$, then

$$\mathcal{RS}[u_L, u_R](\nu) \doteq \begin{cases} u_L & \text{if } \nu < \lambda_{w_{L,R}}(\rho_L), \\ \mathcal{R}_{w_L}(\nu) & \text{if } \lambda_{w_{L,R}}(\rho_L) \leq \nu < \lambda_{w_{L,R}}(\rho_R), \\ u_R & \text{if } \nu \geq \lambda_{w_{L,R}}(\rho_R). \end{cases}$$

(L.4) If $u_L, u_R \in \Omega$ with $w_L \neq w_R$ and $v(u_R) < v(u_L)$, then

$$\mathcal{RS}[u_L, u_R](\nu) \doteq \begin{cases} u_L & \text{if } \nu < s(u_L, u_M), \\ u_M & \text{if } s(u_L, u_M) \leq \nu < v(u_R), \\ u_R & \text{if } \nu \geq v(u_R), \end{cases}$$

where $u_M \doteq (\rho_M, w_M)$ with $\rho_M \doteq p^{-1}(w_L - v(u_R))$ and $w_M \doteq w_L$.

(L.5) If $u_L, u_R \in \Omega$ with $w_L \neq w_R$ and $v(u_L) < v(u_R)$, then

$$\mathcal{RS}[u_L, u_R](\nu) \doteq \begin{cases} u_L & \text{if } \nu < \lambda_{w_L}(\rho_L), \\ \mathcal{R}_{w_L}(\nu) & \text{if } \lambda_{w_L}(\rho_L) \leq \nu < \lambda_{w_L}(\rho_M), \\ u_M & \text{if } \lambda_{w_L}(\rho_M) \leq \nu < v(u_R), \\ u_R & \text{if } \nu \geq v(u_R), \end{cases}$$

where $u_M \doteq (\rho_M, w_M)$ with $\rho_M \doteq p^{-1}([w_L - v(u_R)]_+)$ and $w_M \doteq w_L$.

(L.6) If $u_L = u_R$, then $\mathcal{RS}[u_L, u_R] \doteq u_{L,R}$.

Some comments on the above definition are in order. In case **(L.1)** we have that $\mathcal{RS}[u_L, u_R]$ is the 2-contact discontinuity $\mathcal{C}_2(u_L, u_R)$. In case **(L.2)** we have that $0 \leq \rho_L < \rho_R \leq p^{-1}(w_{L,R})$ and $\mathcal{RS}[u_L, u_R]$ is the 1-shock $\mathcal{S}_1(u_L, u_R)$. In case **(L.3)** we have that $0 \leq \rho_R < \rho_L \leq p^{-1}(w_{L,R})$ and $\mathcal{RS}[u_L, u_R]$ is the 1-rarefaction $\mathcal{R}_1(u_L, u_R)$. In case **(L.4)** we have that

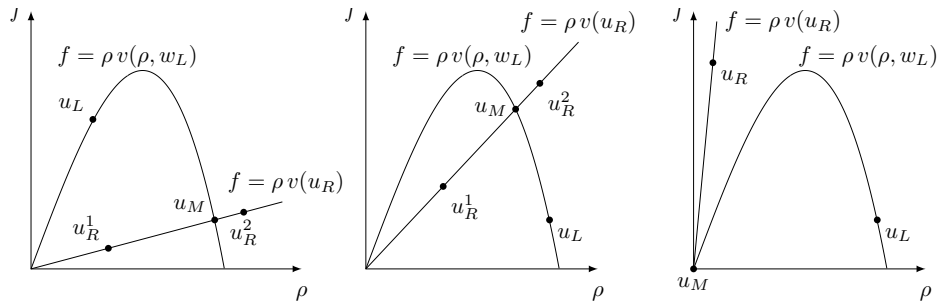

FIGURE 1. Construction of $\mathcal{RS}[u_L, u_R]$ in the cases **(L.4)** and **(L.5)**. Above u_R^1 and u_R^2 represent two possible choices for the right state u_R.

$0 \le \rho_L < \rho_M \le p^{-1}(w_L)$ and $\mathcal{RS}[u_L, u_R]$ is the juxtaposition of $\mathcal{S}_1(u_L, u_M)$ and $\mathcal{C}_2(u_M, u_R)$, see Figure 1. In case **(L.5)** we have that $0 \le \rho_M < \rho_L \le p^{-1}(w_L)$, with $\rho_M = 0$ if and only if $v(u_R) \ge w_L$, and $\mathcal{RS}[u_L, u_R]$ is the juxtaposition of $\mathcal{R}_1(u_L, u_M)$ and $\mathcal{C}_2(u_M, u_R)$, see Figure 1.

We conclude this section with two remarks.

Remark 2.2. According to (2.2), if a vehicle is characterized by the Lagrangian marker w, then it has maximal speed w and length $1/p^{-1}(w)$. Indeed, if the vehicles have the same Lagrangian marker w and are bumper-to-bumper, then their velocity is zero, $v = 0$, and by (2.2) this corresponds to density $\rho = p^{-1}(w)$, hence in any interval with length $L = 1/p^{-1}(w)$ there is $\rho L = 1$ vehicle. This property holds true also for all the proposed generalizations of the ARZ model.

Remark 2.3. We underline that the fundamental diagrams $\{(\rho, f) : f = (w - p(\rho))\,\rho\}$, $w > 0$, do not intersect away from the vacuum. We will see that this property is lost in the following generalizations of the ARZ model.

3. Riemann solver $\mathcal{RS}_{\mathfrak{R}_-,\mathfrak{R}_+}$ for ARZ model with discontinuous flux

Despite the cases that we are going to consider in the next three sections are different, as a matter of fact the three corresponding Riemann solvers obtained as many particle limits can be described in the same way. Roughly speaking, the reason is that all the obtained Riemann solvers optimize the flow at $x = 0$ under some *appropriate* physical restrictions depending on the case under consideration. In this section we first give a general FTL model used to deduce our Riemann solvers and then give a general definition describing them in a unified way.

3.1. Microscopic selection of the Riemann solver $\mathcal{RS}_{\mathfrak{R}_-,\mathfrak{R}_+}$. Choosing a Riemann solver $\mathcal{RS}_{\mathfrak{R}_-,\mathfrak{R}_+} : \Omega^2 \to \mathbf{BV}(\mathbb{R}; \Omega)$ is equivalent to associate

to any $(u_L, u_R) \in \Omega^2$ a unique self-similar weak solution to the Riemann problem (1.1), (1.5). If $\rho_L = 0 = \rho_R$, then we simply define

$$\mathcal{RS}_{\mathfrak{R}_-,\mathfrak{R}_+}[u_L, u_R](\nu) \doteq \begin{cases} u_L & \text{if } \nu < w_R, \\ u_R & \text{if } \nu \geq w_R. \end{cases}$$

Assume now that $\rho_L + \rho_R \neq 0$. We then construct $\mathcal{RS}_{\mathfrak{R}_-,\mathfrak{R}_+}[u_L, u_R]$ as follows. Fix $n \in \mathbb{N}$ and $\delta > 0$. We approximate the Riemann initial condition (1.5) with the truncated Riemann initial condition

$$u(0, x) = u_L \cdot \mathbb{1}_{(-\delta,0)}(x) + u_R \cdot \mathbb{1}_{[0,\delta)}(x). \tag{3.1}$$

As a result, the traffic has *finite* total number of vehicles, that is $\delta\,(\rho_L + \rho_R)$. Define $\ell \doteq \delta\,(\rho_L + \rho_R)/n$. We then introduce basic microscopic interaction rules between the vehicles and encode them in a microscopic FTL model of the form

$$\begin{cases} \dot{\mathtt{x}}_1 = \mathtt{v}(0, \mathtt{w}_1, \bar{\mathtt{x}}_1), & t > 0, \\ \dot{\mathtt{x}}_{i+1} = \mathtt{v}\Big(\frac{\ell}{\mathtt{x}_i - \mathtt{x}_{i+1}}, \mathtt{w}_{i+1}, \mathtt{x}_{i+1}\Big), & t > 0, \quad i \in \{1, \dots, n\}, \\ \mathtt{x}_i(0) = \bar{\mathtt{x}}_i, & \qquad\qquad\; i \in \{1, \dots, n+1\}. \end{cases} \tag{3.2a}$$

Above $\mathtt{x}_i = \mathtt{x}_i(t) \in \mathbb{R}$ is the position at time $t \geq 0$ (of the front bumper) of the i-th vehicle labeled starting from the right. The initial positions $\bar{\mathtt{x}}_1, \dots, \bar{\mathtt{x}}_{n+1}$ are chosen as follows:

$$\begin{aligned} &\rho_L \neq 0 \Longrightarrow \bar{\mathtt{x}}_{i+1} \doteq -\delta + (n-i)\,\frac{\ell}{\rho_L} \leq 0, && i \geq \left\lceil \frac{\rho_R}{\rho_L + \rho_R}\, n \right\rceil, \\ &\rho_L = 0 \Longrightarrow \bar{\mathtt{x}}_{n+1} \doteq 0, \\ &\rho_R \neq 0 \Longrightarrow \bar{\mathtt{x}}_{i+1} \doteq \delta - i\,\frac{\ell}{\rho_R} \geq 0, && i \leq \left\lfloor \frac{\rho_R}{\rho_L + \rho_R}\, n \right\rfloor, \\ &\rho_R = 0 \Longrightarrow \bar{\mathtt{x}}_1 \doteq 0. \end{aligned} \tag{3.2b}$$

The i-th vehicle is characterized by the Lagrangian marker

$$\mathtt{w}_i \doteq \begin{cases} w_L & \text{if } i < N, \\ w_R & \text{if } i \geq N, \end{cases} \qquad N \doteq \left\lceil \frac{\rho_R}{\rho_L + \rho_R}\, n \right\rceil + 1, \tag{3.2c}$$

has maximal speed $\mathtt{w}_i > 0$ and length $\ell / p^{-1}(\mathtt{w}_i)$.

We then associate to (3.2) the approximate discrete density

$$\mathtt{r}(t, x) \doteq \sum_{i=1}^{n} \frac{\ell}{\mathtt{x}_i(t) - \mathtt{x}_{i+1}(t)} \cdot \mathbb{1}_{[\mathtt{x}_{i+1}(t), \mathtt{x}_i(t))}(x) \tag{3.3}$$

and the approximate Lagrangian marker

$$\mathtt{w}(t, x) \doteq w_L \cdot \mathbb{1}_{(-\infty, \mathtt{x}_N(t))}(x) + w_R \cdot \mathbb{1}_{[\mathtt{x}_N(t), +\infty)}(x). \tag{3.4}$$

Notice that for any $t \geq 0$, we have

$$\int_{\mathtt{x}_i(t)}^{\mathtt{x}_{i-1}(t)} \mathtt{r}(t,x)\,\mathrm{d}x = \ell,\ \|\mathtt{r}(t)\|_{\mathbf{L^1}(\mathbb{R})} = \delta\,(\rho_L + \rho_R),\ \mathtt{x}_1(t) = \bar{\mathtt{x}}_1 + \mathtt{v}(0, \mathtt{w}_1, \bar{\mathtt{x}}_1)\,t.$$

At last, by letting $n \to +\infty$ and $\delta \to +\infty$ we expect that $\mathtt{u} \doteq (\mathtt{r}, \mathtt{w})$ converges to a self-similar weak solution $u \doteq (\rho, w)$ to the Riemann problem (1.1), (1.5), and then we accordingly define $\mathcal{RS}_{\mathfrak{R}_-,\mathfrak{R}_+}[u_L, u_R](x/t) \doteq u(t,x)$.

We recall that in the case of a homogeneous road such limit was rigorously proved in [19]. The rigorous proof for the convergence of the discretized solutions $\mathtt{u}$ corresponding to FTL models (3.1), (3.2) considered here is beyond the purposes of the present paper and is left to future works: here we take it for granted. Here we are only interested in showing how it is possible to deduce physically reasonable Riemann solvers from ad hoc computer assisted numerical simulations.

3.2. General definition of Riemann solver $\mathcal{RS}_{\mathfrak{R}_-,\mathfrak{R}_+}$. We recall that the ARZ model can be interpreted as a generalization of the Lighthill–Whitham–Richards model [29, 31]. Indeed, rather than just one (bell shaped) fundamental diagram as for the LWR model, the ARZ model allows to consider a one parameter family of fundamental diagrams $f(\,\cdot\,, w)\colon [0, p^{-1}(w)] \to [0, +\infty)$, $w > 0$, corresponding to the Lax curves of the first family for (2.1). If we consider a non-homogeneous road, then for each road $\mathfrak{R}_\pm$ we consider a corresponding family of fundamental diagrams $\mathsf{f}_\pm(\,\cdot\,, w)\colon [0, p^{-1}(w)] \to [0, +\infty)$, $w > 0$, obtained by applying some *appropriate* physical restrictions. Notice that in this case (2.2) does not hold and cannot be applied to obtain the velocity.

A straightforward adaptation of Definition 2.1 gives the Lax–Riemann solver $\mathcal{RS}_\pm\colon \Omega^2 \to \mathbf{BV}(\mathbb{R}; \Omega)$ corresponding to

$$\begin{cases} \rho_t + \mathsf{f}_\pm(\rho, w)_x = 0, & t > 0,\ x \in \mathbb{R}, \\ w_t + \mathsf{v}_\pm(\rho, w)\, w_x = 0, & t > 0,\ x \in \mathbb{R}, \end{cases}$$

with $\mathsf{f}_\pm(\rho, w) \doteq \rho\, \mathsf{v}_\pm(\rho, w)$. Before giving a general definition for $\mathcal{RS}_{\mathfrak{R}_-,\mathfrak{R}_+}$, we need to introduce some notation. Let $u_* \doteq (\rho_*, w_*)\colon \Omega \times (0, +\infty) \to \Omega$ be defined by

$$\begin{aligned} &w_*(u_R, w_L) \doteq w_L, \\ &\rho_*(u_R, w_L) \doteq \inf\big\{\rho \in [0, p^{-1}(w_L)] : \mathsf{v}_+(\rho, w_L) < \mathsf{v}_+(u_R)\big\}. \end{aligned} \tag{3.5}$$

Assumption (**A.2**) does not ensure that $\mathsf{f}_\pm(\cdot, w)$ attains its maximum

$$\mathsf{F}_\pm(w) \doteq \max_{\rho \in [0, p^{-1}(w)]} \mathsf{f}_\pm(\rho, w) \tag{3.6}$$

at a unique density value. For this reason we introduce

$$\begin{aligned} \mathsf{R}_-(w) &\doteq \min\{\rho \in [0, p^{-1}(w)] : \mathsf{f}_-(\rho, w) = \mathsf{F}_-(w)\}, \\ \mathsf{R}_+(w) &\doteq \max\{\rho \in [0, p^{-1}(w)] : \mathsf{f}_+(\rho, w) = \mathsf{F}_+(w)\}. \end{aligned} \tag{3.7}$$

Define $\mathsf{Q}_- \colon \Omega \to [0, +\infty)$ and $\mathsf{Q}_+ \colon \Omega \times (0, +\infty) \to [0, +\infty)$ as follows:

$$\begin{aligned} \mathsf{Q}_-(u_L) &\doteq \max_{\rho \in [0, p^{-1}(w_L)]} \mathsf{f}_-\big(\mathcal{RS}_-[u_L, (\rho, w_L)](0^-)\big) \\ &= \begin{cases} \mathsf{F}_-(w_L) & \text{if } \rho_L \geq \mathsf{R}_-(w_L), \\ \mathsf{f}_-(u_L) & \text{if } \rho_L < \mathsf{R}_-(w_L), \end{cases} \\ \mathsf{Q}_+(u_R, w_L) &\doteq \max_{\rho \in [0, p^{-1}(w_L)]} \mathsf{f}_+\big(\mathcal{RS}_+[(\rho, w_L), u_*(u_R, w_L)](0^+)\big) \\ &= \begin{cases} \mathsf{f}_+(u_*(u_R, w_L)) & \text{if } \rho_*(u_R, w_L) > \mathsf{R}_+(w_L), \\ \mathsf{F}_+(w_L) & \text{if } \rho_*(u_R, w_L) \leq \mathsf{R}_+(w_L). \end{cases} \end{aligned} \tag{3.8}$$

Let then $\hat{u} \doteq (\hat{\rho}, \hat{w}), \check{u} \doteq (\check{\rho}, \check{w}) \colon \Omega^2 \to \Omega$ be defined by

$$\begin{cases} \hat{\rho}(u_L, u_R) \doteq \max\big\{\rho \in \big[\mathsf{R}_-(w_L), p^{-1}(w_L)\big] : \mathsf{f}_-(\rho, w_L) = \mathsf{Q}(u_L, u_R)\big\}, \\ \hat{w}(u_L, u_R) = w_L, \end{cases} \tag{3.9}$$

$$\begin{cases} \check{\rho}(u_L, u_R) \doteq \min\{\rho \in [0, \mathsf{R}_+(w_L)] : \mathsf{f}_+(\rho, w_L) = \mathsf{Q}(u_L, u_R)\}, \\ \check{w}(u_L, u_R) = w_L, \end{cases} \tag{3.10}$$

where

$$\mathsf{Q}(u_L, u_R) \doteq \min\{\mathsf{Q}_-(u_L), \mathsf{Q}_+(u_R, w_L)\}. \tag{3.11}$$

We are now in the position to give the following definition.

Definition 3.1. The Riemann solver $\mathcal{RS}_{\mathfrak{R}_-, \mathfrak{R}_+} \colon \Omega^2 \to \mathbf{BV}(\mathbb{R}; \Omega)$ for (1.1), (1.2), (1.3) is defined as follows:

$$\mathcal{RS}_{\mathfrak{R}_-, \mathfrak{R}_+}[u_L, u_R](\nu) \doteq \begin{cases} \mathcal{RS}_-[u_L, \hat{u}(u_L, u_R)](\nu) & \text{if } \nu < 0, \\ \mathcal{RS}_+[\check{u}(u_L, u_R), u_R](\nu) & \text{if } \nu \geq 0. \end{cases}$$

In Sections 4, 5, and 6, we assume that the road sections $\mathfrak{R}_\pm$ are characterized by either different capacities $F_\pm$, or speed limits $V_\pm$, or both capacities and speed limits. In other words, we consider a traffic along the road $\mathbb{R}$ governed by (1.1), (1.2) and satisfying one of the following constraints:

Section 4	$\mathsf{f}(u(t,x), x) \leq F_- \cdot \mathbb{1}_{\mathfrak{R}_-}(x) + F_+ \cdot \mathbb{1}_{\mathfrak{R}_+}(x)$,
Section 5	$\mathsf{v}(u(t,x), x) \leq V_- \cdot \mathbb{1}_{\mathfrak{R}_-}(x) + V_+ \cdot \mathbb{1}_{\mathfrak{R}_+}(x)$,
Section 6	$\begin{cases} \mathsf{f}(u(t,x), x) \leq F_- \cdot \mathbb{1}_{\mathfrak{R}_-}(x) + F_+ \cdot \mathbb{1}_{\mathfrak{R}_+}(x), \\ \mathsf{v}(u(t,x), x) \leq V_- \cdot \mathbb{1}_{\mathfrak{R}_-}(x) + V_+ \cdot \mathbb{1}_{\mathfrak{R}_+}(x). \end{cases}$

If the fundamental diagram $\rho \mapsto f(\rho, w)$ satisfies the constraint under consideration along the road section $\mathfrak{R}_-$, then we simply set $\mathsf{f}_-(\cdot, w, x) \equiv f(\cdot, w)$ for any $x \in \mathfrak{R}_-$; analogously in $\mathfrak{R}_+$. For the remaining cases we propose two approaches: if $\rho \mapsto f(\rho, w)$ does not satisfy the constraint under consideration, then, roughly speaking, either we "rescale" it by a coefficient, or simply "cut" the "bad" part. The first approach resembles that proposed in [18] for a scalar conservation law with a point constraint on the flow; the second approach is analogous to that proposed in [12] for a scalar conservation law with different velocity constraints along two sections of a road. We apply the first approach in Subsections 4.1, 5.1, and 6.1, whereas the second approach will be exploited in Subsections 4.2, 5.2, and 6.2.

We conclude this section with some remarks.

Remark 3.2. The introduction of $\mathsf{R}_\pm$ is needed in order to properly define $\mathsf{Q}_\pm$, $\hat{u}$ and $\check{u}$ in (3.8), (3.9), and (3.10), respectively. We stress that in this respect, commuting min with max in (3.7) does not affect such definitions, hence also that of Q in (3.11).

Remark 3.3. We stress that $\mathcal{RS}_{\mathfrak{R}_-,\mathfrak{R}_+}$ given in Definition 3.1 is a Riemann solver, namely for any $(u_L, u_R) \in \Omega^2$ we have that

$$u(t,x) \doteq \mathcal{RS}_{\mathfrak{R}_-,\mathfrak{R}_+}[u_L, u_R](x/t)$$

is a weak solution. This simply follows from the fact that $\mathcal{RS}_\pm$ are Riemann solvers and by the fact that by (3.9), (3.10) we have $\mathsf{f}_-(\hat{u}(u_L, u_R)) = \mathsf{f}_+(\check{u}(u_L, u_R))$.

Remark 3.4. Definition 3.1 is analogous to that given in [18] for point constraint on the flow. The main difference is that here we do not distinguish between the classical and non-classical cases. The reason is that we want to highlight that both the classical and non-classical solutions optimize the flow through $x = 0$ under some *appropriate* physical restrictions, depending on the case under consideration.

Remark 3.5. The characteristics of the road do not affect the length of the vehicles. For this reason we always assume that $\mathsf{f}_\pm(\rho, w) = 0$ if and only if $\rho \in \{0, p^{-1}(w)\}$.

Remark 3.6. For any $(u_L, u_R) \in \Omega^2$ such that $w_L \neq w_R$ we have that the right most wave of $\mathcal{RS}_{\mathfrak{R}_-,\mathfrak{R}_+}[u_L, u_R]$ is a contact discontinuity with speed of propagation $\mathsf{v}_+(u_R)$. We stress that 2-contact discontinuities always separate the two families of vehicles, characterized by the Lagrangian markers w_L and w_R.

Remark 3.7. We will see that $\nu \mapsto \mathcal{RS}_{\mathfrak{R}_-,\mathfrak{R}_+}(\nu)$ may have total variation greater than that of the initial datum, namely $|\rho_L - \rho_R| + |w_L - w_R|$; moreover, the maximum principle holds for the w-coordinate but may fail for the ρ-coordinates.

Remark 3.8. The simplest choice for $\mathsf{f}_\pm$ satisfying the constraint under consideration is to rescale $f(\cdot, w)$ for any $w > 0$. However, with such choice there is no need to study the resulting model as it is a straightforward generalization of the ARZ model.

4. ARZ model for two roads with different capacities

In this section we assume that the two roads $\mathfrak{R}_- \doteq (-\infty, 0)$ and $\mathfrak{R}_+ \doteq [0, +\infty)$ have capacities $F_- > 0$ and $F_+ > 0$, respectively. Then the evolution of traffic along $\mathbb{R}$ can be described by (1.1), (1.3), (1.4) with $\mathsf{f}_\pm \colon \Omega \to [0, +\infty)$ such that

$$\mathsf{f}_\pm(u) \le F_\pm \text{ for any } u \in \Omega \iff \mathsf{F}_\pm(w) \le F_\pm \text{ for any } w > 0, \tag{4.1}$$

where $\mathsf{F}_\pm(w)$ is defined in (3.6).

Let f be defined by (2.3) and introduce the following notation

$$\begin{aligned} &R(w) \doteq \mathcal{R}_w(0),\ F(w) \doteq \max_{\rho \in [0, p^{-1}(w)]} f(\rho, w) = f(R(w), w),\\ &W_\pm \doteq F^{-1}(F_\pm). \end{aligned} \tag{4.2}$$

Remark 4.1. Notice that if $p(\rho) \doteq \rho^\gamma$, $\gamma > 0$, then

$$R(w) \doteq \left(\frac{w}{\gamma+1}\right)^{\frac{1}{\gamma}},\ F(w) \doteq \gamma\left(\frac{w}{\gamma+1}\right)^{1+\frac{1}{\gamma}},\ W_\pm \doteq (\gamma+1)\left(\frac{F_\pm}{\gamma}\right)^{\frac{\gamma}{\gamma+1}}. \tag{4.3}$$

The fundamental diagram $\rho \mapsto f(\rho, w)$ fails to satisfy (4.1) if and only if

$$F(w) > F_\pm \iff w > W_\pm.$$

For this reason we necessarily have $\mathsf{f}_\pm(\cdot, w) \not\equiv f(\cdot, w)$ for all $w > W_\pm$.

In the following two subsections, we propose two possible choices for the fluxes $\mathsf{f}_\pm$ satisfying (4.1) and such that $\mathsf{f}_\pm(\cdot, w) \equiv f(\cdot, w)$ for all $w \le W_\pm$.

4.1. First option.

In this subsection, we consider problem (1.1), (1.3), (1.4) with

$$\begin{aligned} &\mathsf{v}_\pm(\rho, w) \doteq \frac{\min\{F_\pm, F(w)\}}{F(w)}\, v(\rho, w) = \begin{cases} v(\rho, w) & \text{if } w \le W_\pm,\\ \frac{F_\pm}{F(w)}\, v(\rho, w) & \text{if } w > W_\pm, \end{cases}\\ &\mathsf{f}_\pm(u) \doteq \rho \cdot \mathsf{v}_\pm(u), \end{aligned} \tag{4.4}$$

where v is defined in $(2.3)_1$. Notice that both the fundamental diagram $\rho \mapsto f(\rho, w)$ and the "rescaled" fundamental diagrams $\rho \mapsto \mathsf{f}_\pm(\rho, w)$ attain their maximal values at $R(w) \doteq \mathcal{R}_w(0)$, therefore both $\mathsf{R}_\pm$ given in (3.7) simply reduce to R defined in $(4.2)_1$, namely $\mathsf{R}_\pm(w) = R(w)$. In particular

$$f(R(w), w) = F(w) \ge \mathsf{f}_\pm(R(w), w) = \begin{cases} F(w) & \text{if } w \le W_\pm,\\ F_\pm & \text{if } w > W_\pm, \end{cases}$$

and clearly $\mathsf{f}_\pm$ satisfies (4.1). In the present case the maps $\mathsf{Q}_\pm\colon \Omega\times(0,+\infty)\to[0,+\infty)$ defined in (3.8) become

$$\mathsf{Q}_-(u_L)\doteq\begin{cases}\mathsf{f}_-(u_L) & \text{if } \rho_L\le R(w_L),\\ F(w_L) & \text{if } \rho_L> R(w_L) \text{ and } w\le W_-,\\ F_- & \text{if } \rho_L> R(w_L) \text{ and } w> W_-,\end{cases}$$

$$\mathsf{Q}_+(u_R,w_L)\doteq\begin{cases}F(w_L) & \text{if } \rho_*(u_R,w_L)\le R(w_L) \text{ and } w\le W_+,\\ F_+ & \text{if } \rho_*(u_R,w_L)\le R(w_L) \text{ and } w> W_+,\\ \mathsf{f}_+(u_*(u_R,w_L)) & \text{if } \rho_*(u_R,w_L)> R(w_L),\end{cases}$$

where $u_*\doteq(\rho_*,w_*)$ is defined in (3.5).

We run computer assisted numerical simulations of the FTL model (3.2), (4.4) with $p(\rho)\doteq\rho^\gamma$, $\gamma\doteq 2$. The outputs of some simulations are presented in Figures 2–7 and show a good agreement with the Riemann solver $\mathcal{RS}_{\mathfrak{R}_-,\mathfrak{R}_+}$ for (1.1), (1.3), (1.4), (4.4) given in Definition 3.1, at least in the cases under consideration.

We construct below $\mathcal{RS}_{\mathfrak{R}_-,\mathfrak{R}_+}[u_L,u_R]$ for the cases considered in Figures 2–7, with the aim to make Definition 3.1 more clear. We mainly focus on computing $\mathsf{Q}(u_L,u_R)$, because then it is easy to get $\hat u(u_L,u_R)$ and $\check u(u_L,u_R)$. At last we describe $\mathcal{RS}_-[u_L,\hat u(u_L,u_R)]$ and $\mathcal{RS}_+[\check u(u_L,u_R),u_R]$ because then it is easy to construct $\mathcal{RS}_{\mathfrak{R}_-,\mathfrak{R}_+}[u_L,u_R]$ by applying Definition 3.1. For simplicity, below we use the following notation

$$\hat u=\hat u(u_L,u_R),\qquad \check u=\check u(u_L,u_R),\qquad u_*=u_*(u_R,w_L). \tag{4.5}$$

(F1.a) For an initial datum as in Figure 2, we have

$$\left.\begin{aligned}\rho_L>\mathsf{R}_-(w_L)&\implies \mathsf{Q}_-(u_L)=\mathsf{F}_-(w_L)\\ \rho_*>\mathsf{R}_+(w_L)&\implies \mathsf{Q}_+(u_R,w_L)=\mathsf{f}_+(u_*)\end{aligned}\right\}\implies \mathsf{Q}(u_L,u_R)=\mathsf{f}_+(u_*).$$

$\mathcal{RS}_-[u_L,\hat u]$ is the 1-rarefaction $\mathcal{R}_1(u_L,\hat u)$, and $\mathcal{RS}_+[\check u,u_R]$ is the juxtaposition of the 1-shock $\mathcal{S}_1(\check u,u_*)$ and the 2-contact discontinuity $\mathcal{C}_2(u_*,u_R)$. $\mathcal{S}_1(\check u,u_*)$ is *stationary* and for this reason the ρ-component of $\mathcal{RS}_{\mathfrak{R}_-,\mathfrak{R}_+}[u_L,u_R]$ does not attain the value $\check\rho$.

(F1.b) For an initial datum as in Figure 3, we have

$$\left.\begin{aligned}\rho_L<\mathsf{R}_-(w_L)&\implies \mathsf{Q}_-(u_L)=\mathsf{f}_-(u_L)\\ \rho_*>\mathsf{R}_+(w_L)&\implies \mathsf{Q}_+(u_R,w_L)=\mathsf{f}_+(u_*)\end{aligned}\right\}\implies \mathsf{Q}(u_L,u_R)=\mathsf{f}_-(u_L).$$

$\mathcal{RS}_-[u_L,\hat u]$ is the 1-shock $\mathcal{S}_1(u_L,\hat u)$, and $\mathcal{RS}_+[\check u,u_R]$ is the juxtaposition of the 1-shock $\mathcal{S}_1(\check u,u_*)$ and the 2-contact discontinuity $\mathcal{C}_2(u_*,u_R)$. $\mathcal{S}_1(u_L,\hat u)$ is *stationary* and for this reason the ρ-component of $\mathcal{RS}_{\mathfrak{R}_-,\mathfrak{R}_+}[u_L,u_R]$ does not attain the value $\hat\rho$.

(F1.c) For an initial datum as in Figure 4, we have

$$\left.\begin{aligned}\rho_L<\mathsf{R}_-(w_L)&\implies \mathsf{Q}_-(u_L)=\mathsf{f}_-(u_L)\\ \rho_*<\mathsf{R}_+(w_L)&\implies \mathsf{Q}_+(u_R,w_L)=\mathsf{F}_+(w_L)=F_+\end{aligned}\right\}\implies \mathsf{Q}(u_L,u_R)=F_+.$$

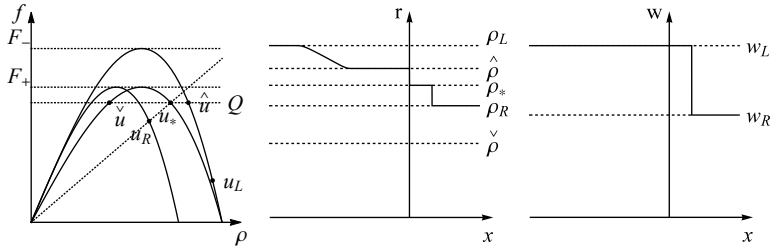

FIGURE 2. The approximate density (3.3), center, and approximate Lagrangian marker (3.4), right, corresponding to FTL model (3.2), (4.4) and the initial datum $(u_L, u_R) \in \Omega^2$, left. The solution obtained by applying the Riemann solver $\mathcal{RS}_{\mathfrak{R}_-,\mathfrak{R}_+}$ is described in **(F1.a)**.

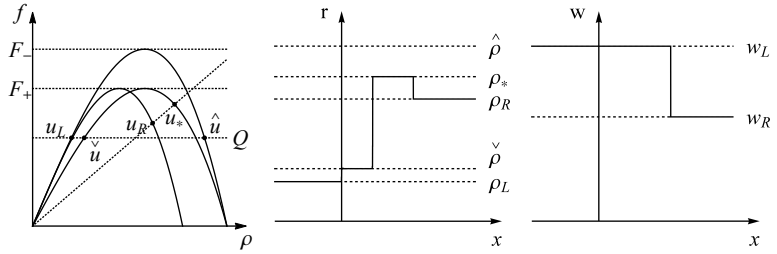

FIGURE 3. The approximate density (3.3), center, and approximate Lagrangian marker (3.4), right, corresponding to FTL model (3.2), (4.4) and the initial datum $(u_L, u_R) \in \Omega^2$, left. The solution obtained by applying the Riemann solver $\mathcal{RS}_{\mathfrak{R}_-,\mathfrak{R}_+}$ is described in **(F1.b)**.

$\mathcal{RS}_-[u_L, \hat{u}]$ is the 1-shock $\mathcal{S}_1(u_L, \hat{u})$, and $\mathcal{RS}_+[\check{u}, u_R]$ is the juxtaposition of the 1-rarefaction $\mathcal{R}_1(\check{u}, u_*)$ and the 2-contact discontinuity $\mathcal{C}_2(u_*, u_R)$.

(F1.d) For an initial datum as in Figure 5, we have

$$\left.\begin{array}{rcl} \rho_L > \mathsf{R}_-(w_L) & \Longrightarrow & \mathsf{Q}_-(u_L) = \mathsf{F}_-(w_L) = F_- \\ \rho_* < \mathsf{R}_+(w_L) & \Longrightarrow & \mathsf{Q}_+(u_R, w_L) = \mathsf{F}_+(w_L) = F_+ \end{array}\right\} \Longrightarrow \mathsf{Q}(u_L, u_R) = F_+.$$

$\mathcal{RS}_-[u_L, \hat{u}]$ is the 1-rarefaction $\mathcal{R}_1(u_L, \hat{u})$, and $\mathcal{RS}_+[\check{u}, u_R]$ is the juxtaposition of the 1-rarefaction $\mathcal{R}_1(\check{u}, u_*)$ and the 2-contact discontinuity $\mathcal{C}_2(u_*, u_R)$. Notice that $\mathsf{v}_+(u_R) > w_L$ and for this reason $\rho_* = 0$.

(F1.e) For an initial datum as in Figure 6, we have

$$\left.\begin{array}{rcl} \rho_L > \mathsf{R}_-(w_L) & \Longrightarrow & \mathsf{Q}_-(u_L) = \mathsf{F}_-(w_L) = F_- \\ \rho_* > \mathsf{R}_+(w_L) & \Longrightarrow & \mathsf{Q}_+(u_R, w_L) = \mathsf{f}_+(u_*) \end{array}\right\} \Longrightarrow \mathsf{Q}(u_L, u_R) = F_-.$$

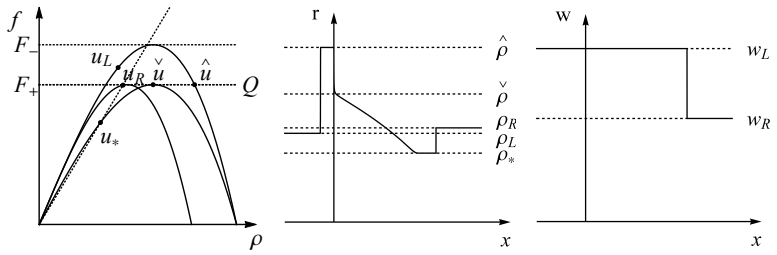

FIGURE 4. The approximate density (3.3), center, and approximate Lagrangian marker (3.4), right, corresponding to FTL model (3.2), (4.4) and the initial datum $(u_L, u_R) \in \Omega^2$, left. The solution obtained by applying the Riemann solver $\mathcal{RS}_{\mathfrak{R}_-,\mathfrak{R}_+}$ is described in **(F1.c)**.

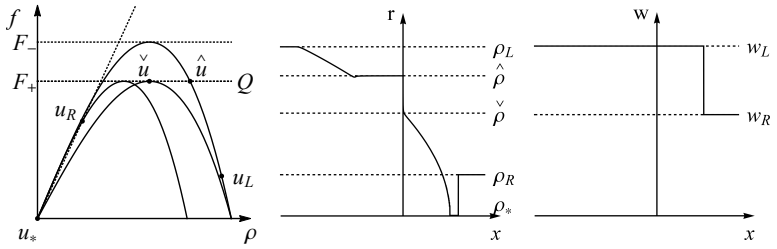

FIGURE 5. The approximate density (3.3), center, and approximate Lagrangian marker (3.4), right, corresponding to FTL model (3.2), (4.4) and the initial datum $(u_L, u_R) \in \Omega^2$, left. The solution obtained by applying the Riemann solver $\mathcal{RS}_{\mathfrak{R}_-,\mathfrak{R}_+}$ is described in **(F1.d)**.

$\mathcal{RS}_-[u_L, \hat{u}]$ is the 1-rarefaction $\mathcal{R}_1(u_L, \hat{u})$, and $\mathcal{RS}_+[\check{u}, u_R]$ is the juxtaposition of the 1-shock $\mathcal{S}_1(\check{u}, u_*)$ and the 2-contact discontinuity $\mathcal{C}_2(u_*, u_R)$.

(F1.f) For an initial datum as in Figure 7, we have

$$\left.\begin{array}{rl} \rho_L > \mathsf{R}_-(w_L) & \Longrightarrow \quad \mathsf{Q}_-(u_L) = \mathsf{F}_-(w_L) = F_- \\ \rho_* < \mathsf{R}_+(w_L) & \Longrightarrow \mathsf{Q}_+(u_R, w_L) = \mathsf{F}_+(w_L) = F_+ \end{array}\right\} \Longrightarrow \mathsf{Q}(u_L, u_R) = F_-.$$

$\mathcal{RS}_-[u_L, \hat{u}]$ is the 1-rarefaction $\mathcal{R}_1(u_L, \hat{u})$, and $\mathcal{RS}_+[\check{u}, u_R]$ is the juxtaposition of the 1-rarefaction $\mathcal{R}_1(\check{u}, u_*)$ and the 2-contact discontinuity $\mathcal{C}_2(u_*, u_R)$. Notice that $\mathsf{v}_+(u_R) > w_L$ and for this reason $\rho_* = 0$.

We conclude this subsection with the following remark.

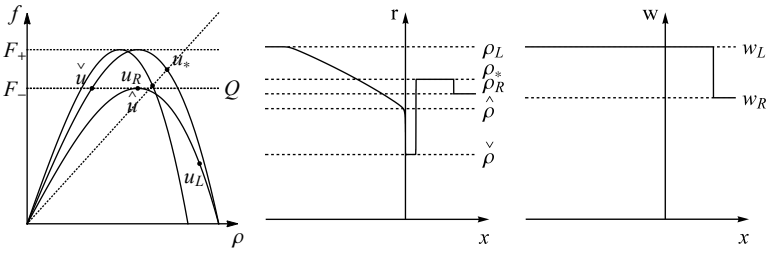

FIGURE 6. The approximate density (3.3), center, and approximate Lagrangian marker (3.4), right, corresponding to FTL model (3.2), (4.4) and the initial datum $(u_L, u_R) \in \Omega^2$, left. The solution obtained by applying the Riemann solver $\mathcal{RS}_{\mathfrak{R}_-,\mathfrak{R}_+}$ is described in **(F1.e)**.

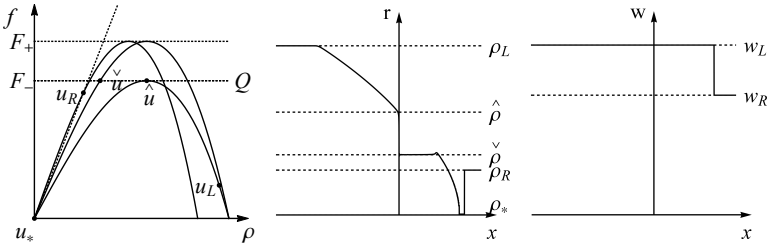

FIGURE 7. The approximate density (3.3), center, and approximate Lagrangian marker (3.4), right, corresponding to FTL model (3.2), (4.4) and the initial datum $(u_L, u_R) \in \Omega^2$, left. The solution obtained by applying the Riemann solver $\mathcal{RS}_{\mathfrak{R}_-,\mathfrak{R}_+}$ is described in **(F1.f)**.

Remark 4.2. The velocity functions (4.4) imply that along $\mathfrak{R}_\pm$ a vehicle with the Lagrangian marker $w > 0$ has maximal speed

$$v_\pm(0, w) = \begin{cases} w & \text{if } w \le W_\pm, \\ \frac{F_\pm}{F(w)}\, w & \text{if } w > W_\pm. \end{cases}$$

As a consequence, the capacities of the road sections affect the maximal speed of only the fast vehicles. Yet high speed vehicles may be almost "blocked". Indeed, we have $\lim_{w\to+\infty} \frac{w}{F(w)} = 0$, see for instance $(4.3)_2$ for the case $p(\rho) = \rho^\gamma$, $\gamma > 0$. A possible realistic motivation is that the capacities of the road sections are mainly linked to the quality of the road surface. It is then reasonable to assume that, in poor words, the change in the quality of the road surface (e.g., from asphalt to terrain) does not affect very slow heavy trucks, e.g., a bulldozer, while it deeply affects the performance of race cars, e.g., a Ferrari 599 GTO. In this respect, the second

approach seems more reasonable when the change in the quality of road surface is not "drastic", see Subsection 4.2.

4.2. Second option. Motivated by Remark 4.2, in this subsection, we consider

$$\mathsf{v}_\pm(\rho,w) \doteq \begin{cases} F_\pm/\rho & \text{if } w > W_\pm \text{ and } f(\rho,w) > F_\pm, \\ v(\rho,w) & \text{otherwise,} \end{cases} \tag{4.6}$$
$$\mathsf{f}_\pm(\rho,w) \doteq \rho\,\mathsf{v}_\pm(\rho,w),$$

where v is defined in $(2.3)_1$. Clearly $\mathsf{f}_\pm$ satisfies (4.1). The above choice for $\mathsf{f}_\pm$ is motivated as follows: the capacity $F_\pm$ of the road $\mathfrak{R}_\pm$ has an effect on the traffic only when it is achieved.

We run computer assisted numerical simulations of the FTL model (3.2), (4.6) with $p(\rho) \doteq \rho^\gamma$, $\gamma \doteq 2$. The outputs of some simulations are presented in Figures 8–13 and show a good agreement with the Riemann solver $\mathcal{RS}_{\mathfrak{R}_-,\mathfrak{R}_+}$ for (1.1), (1.3), (1.4), (4.6) given in Definition 3.1, at least in the cases under consideration.

We construct below $\mathcal{RS}_{\mathfrak{R}_-,\mathfrak{R}_+}[u_L,u_R]$ for the cases considered in Figures 8–13, with the aim to make Definition 3.1 more clear. For simplicity, below we use the notation introduced in (4.5).

(F2.a) For an initial datum as in Figure 8, we have

$$\left.\begin{array}{rcl} \rho_L > \mathsf{R}_-(w_L) & \Longrightarrow & \mathsf{Q}_-(u_L) = \mathsf{F}_-(w_L) = F_- \\ \rho_* > \mathsf{R}_+(w_L) & \Longrightarrow & \mathsf{Q}_+(u_R,w_L) = \mathsf{f}_+(u_*) \end{array}\right\} \Longrightarrow \mathsf{Q}(u_L,u_R) = F_-.$$

$\mathcal{RS}_-[u_L,\hat{u}]$ is the 1-rarefaction $\mathcal{R}_1(u_L,\hat{u})$, and $\mathcal{RS}_+[\check{u},u_R]$ is the juxtaposition of the 1-shock $\mathcal{S}_1(\check{u},u_*)$ and the 2-contact discontinuity $\mathcal{C}_2(u_*,u_R)$.

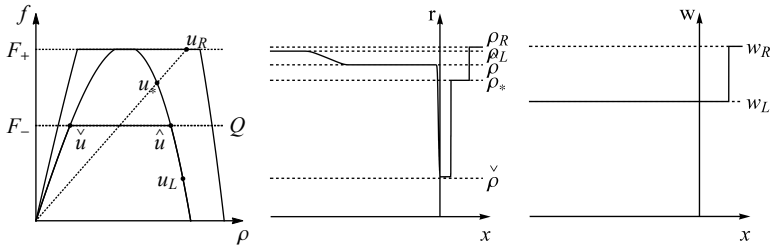

FIGURE 8. The approximate density (3.3), center, and approximate Lagrangian marker (3.4), right, corresponding to FTL model (3.2), (4.6) and the initial datum $(u_L,u_R) \in \Omega^2$, left. The solution obtained by applying the Riemann solver $\mathcal{RS}_{\mathfrak{R}_-,\mathfrak{R}_+}$ is described in **(F2.a)**.

(F2.b) For an initial datum as in Figure 9, we have

$$\left.\begin{array}{rl} \rho_L > \mathsf{R}_-(w_L) & \Longrightarrow \mathsf{Q}_-(u_L) = \mathsf{F}_-(w_L) = F_- \\ \rho_* > \mathsf{R}_+(w_L) & \Longrightarrow \quad \mathsf{Q}_+(u_R, w_L) = \mathsf{f}_+(u_*) \end{array}\right\} \Longrightarrow \mathsf{Q}(u_L, u_R) = F_-.$$

$\mathcal{RS}_-[u_L, \hat{u}]$ is the 1-contact discontinuity $\mathcal{C}_1(u_L, \hat{u})$, and $\mathcal{RS}_+[\check{u}, u_R]$ is the juxtaposition of the 1-shock $\mathcal{S}_1(\check{u}, u_*)$ and the 2-contact discontinuity $\mathcal{C}_2(u_*, u_R)$. $\mathcal{C}_1(u_L, \hat{u})$ is *stationary* and for this reason the ρ-component of $\mathcal{RS}_{\mathfrak{R}_-,\mathfrak{R}_+}[u_L, u_R]$ does not attain the value $\hat{\rho}$.

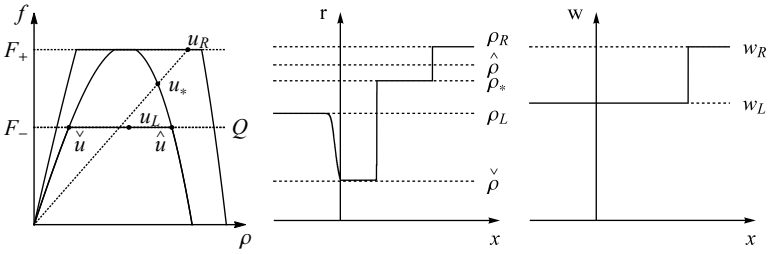

FIGURE 9. The approximate density (3.3), center, and approximate Lagrangian marker (3.4), right, corresponding to FTL model (3.2), (4.6) and the initial datum $(u_L, u_R) \in \Omega^2$, left. The solution obtained by applying the Riemann solver $\mathcal{RS}_{\mathfrak{R}_-,\mathfrak{R}_+}$ is described in **(F2.b)**.

(F2.c) For an initial datum as in Figure 10, we have

$$\left.\begin{array}{rl} \rho_L > \mathsf{R}_-(w_L) & \Longrightarrow \mathsf{Q}_-(u_L) = \mathsf{F}_-(w_L) = F_- \\ \rho_* > \mathsf{R}_+(w_L) & \Longrightarrow \quad \mathsf{Q}_+(u_R, w_L) = \mathsf{f}_+(u_*) \end{array}\right\} \Longrightarrow \mathsf{Q}(u_L, u_R) = \mathsf{f}_+(u_*).$$

$\mathcal{RS}_-[u_L, \hat{u}]$ is the 1-rarefaction $\mathcal{R}_1(u_L, \hat{u})$, and $\mathcal{RS}_+[\check{u}, u_R]$ is the juxtaposition of the 1-shock $\mathcal{S}_1(\check{u}, u_*)$ and the 2-contact discontinuity $\mathcal{C}_2(u_*, u_R)$. $\mathcal{S}_1(\check{u}, u_*)$ is *stationary* and for this reason the ρ-component of $\mathcal{RS}_{\mathfrak{R}_-,\mathfrak{R}_+}[u_L, u_R]$ does not attain the value $\check{\rho}$. Notice that $\hat{u} = u_*$.

(F2.d) For an initial datum as in Figure 11, we have

$$\left.\begin{array}{rl} \rho_L > \mathsf{R}_-(w_L) & \Longrightarrow \quad \mathsf{Q}_-(u_L) = \mathsf{F}_-(w_L) = F_- \\ \rho_* < \mathsf{R}_+(w_L) & \Longrightarrow \mathsf{Q}_+(u_R, w_L) = \mathsf{F}_+(w_L) = F_+ \end{array}\right\} \Longrightarrow \mathsf{Q}(u_L, u_R) = F_-.$$

$\mathcal{RS}_-[u_L, \hat{u}]$ is the 1-contact discontinuity $\mathcal{C}_1(u_L, \hat{u})$, and $\mathcal{RS}_+[\check{u}, u_R]$ is the juxtaposition of the 1-shock $\mathcal{S}_1(\check{u}, u_*)$ and the 2-contact discontinuity $\mathcal{C}_2(u_*, u_R)$. $\mathcal{C}_1(u_L, \hat{u})$ is *stationary* and for this reason the ρ-component of $\mathcal{RS}_{\mathfrak{R}_-,\mathfrak{R}_+}[u_L, u_R]$ does not attain the value $\hat{\rho}$.

(F2.e) For an initial datum as in Figure 12, we have

$$\left.\begin{array}{rl} \rho_L > \mathsf{R}_-(w_L) & \Longrightarrow \quad \mathsf{Q}_-(u_L) = \mathsf{F}_-(w_L) = F_- \\ \rho_* < \mathsf{R}_+(w_L) & \Longrightarrow \mathsf{Q}_+(u_R, w_L) = \mathsf{F}_+(w_L) = F_+ \end{array}\right\} \Longrightarrow \mathsf{Q}(u_L, u_R) = F_+.$$

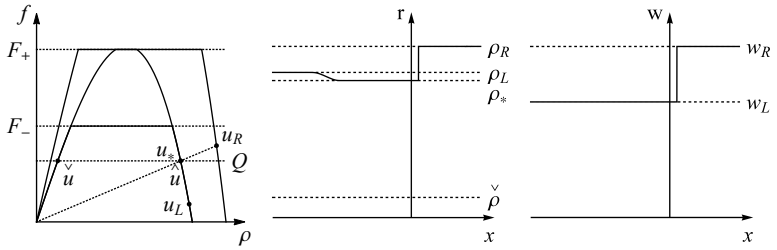

FIGURE 10. The approximate density (3.3), center, and approximate Lagrangian marker (3.4), right, corresponding to FTL model (3.2), (4.6) and the initial datum $(u_L, u_R) \in \Omega^2$, left. The solution obtained by applying the Riemann solver $\mathcal{RS}_{\mathfrak{R}_-,\mathfrak{R}_+}$ is described in **(F2.c)**.

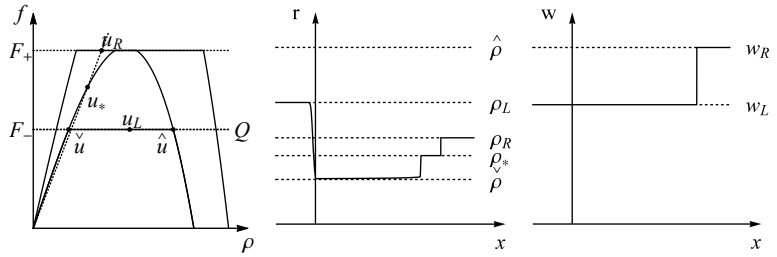

FIGURE 11. The approximate density (3.3), center, and approximate Lagrangian marker (3.4), right, corresponding to FTL model (3.2), (4.6) and the initial datum $(u_L, u_R) \in \Omega^2$, left. The solution obtained by applying the Riemann solver $\mathcal{RS}_{\mathfrak{R}_-,\mathfrak{R}_+}$ is described in **(F2.d)**.

$\mathcal{RS}_-[u_L, \hat{u}]$ is the 1-shock $\mathcal{S}_1(u_L, \hat{u})$, and $\mathcal{RS}_+[\check{u}, u_R]$ is the juxtaposition of the 1-contact discontinuity $\mathcal{C}_1(\check{u}, u_*)$ and the 2-contact discontinuity $\mathcal{C}_2(u_*, u_R)$. $\mathcal{C}_1(\check{u}, u_*)$ is *stationary* and for this reason the ρ-component of $\mathcal{RS}_{\mathfrak{R}_-,\mathfrak{R}_+}[u_L, u_R]$ does not attain the value $\check{\rho}$. Notice that $\rho_* = \rho_R$ but $w_* \neq w_R$.

(F2.f) For an initial datum as in Figure 13, we have

$$\left.\begin{array}{rcl} \rho_L > \mathsf{R}_-(w_L) & \Longrightarrow & \mathsf{Q}_-(u_L) = \mathsf{F}_-(w_L) = F_- \\ \rho_* < \mathsf{R}_+(w_L) & \Longrightarrow & \mathsf{Q}_+(u_R, w_L) = \mathsf{F}_+(w_L) = F_+ \end{array}\right\} \Longrightarrow \mathsf{Q}(u_L, u_R) = F_+.$$

$\mathcal{RS}_-[u_L, \hat{u}]$ is the 1-shock $\mathcal{S}_1(u_L, \hat{u})$, and $\mathcal{RS}_+[\check{u}, u_R]$ is the juxtaposition of the 1-contact discontinuity $\mathcal{C}_1(\check{u}, u_*)$ and the 2-contact discontinuity $\mathcal{C}_2(u_*, u_R)$. $\mathcal{C}_1(\check{u}, u_*)$ is *stationary* and for this reason the ρ-component of $\mathcal{RS}_{\mathfrak{R}_-,\mathfrak{R}_+}[u_L, u_R]$ does not attain the value $\check{\rho}$.

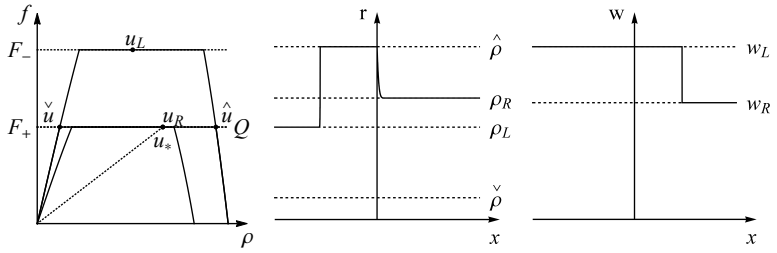

FIGURE 12. The approximate density (3.3), center, and approximate Lagrangian marker (3.4), right, corresponding to FTL model (3.2), (4.6) and the initial datum $(u_L, u_R) \in \Omega^2$, left. The solution obtained by applying the Riemann solver $\mathcal{RS}_{\mathfrak{R}_-,\mathfrak{R}_+}$ is described in **(F2.e)**.

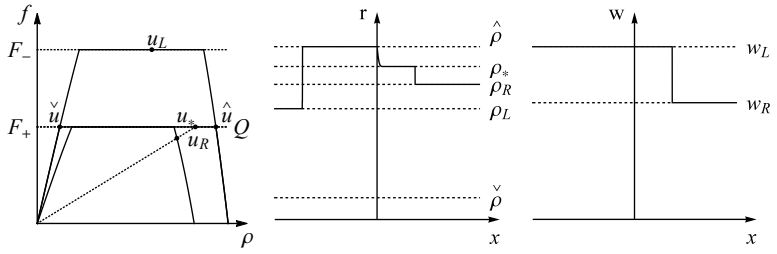

FIGURE 13. The approximate density (3.3), center, and approximate Lagrangian marker (3.4), right, corresponding to FTL model (3.2), (4.6) and the initial datum $(u_L, u_R) \in \Omega^2$, left. The solution obtained by applying the Riemann solver $\mathcal{RS}_{\mathfrak{R}_-,\mathfrak{R}_+}$ is described in **(F2.f)**.

5. ARZ model for two roads with different speed limits

In this section, we consider two roads $\mathfrak{R}_- \doteq (-\infty, 0)$ and $\mathfrak{R}_+ \doteq [0, +\infty)$ with speed limits $V_- > 0$ and $V_+ > 0$, respectively. Then the evolution of traffic along $\mathbb{R}$ can be described by (1.1), (1.3), (1.4) with $\mathsf{v}_\pm \colon \Omega \to [0, +\infty)$ such that

$$\mathsf{v}_\pm(u) \le V_\pm \text{ for any } u \in \Omega \iff \mathsf{v}_\pm(0, w) \le V_\pm \text{ for any } w > 0. \tag{5.1}$$

The velocity map $\rho \mapsto v(\rho, w)$ fails to satisfy (5.1) if and only if

$$v(0, w) > V_\pm \iff w > V_\pm.$$

For this reason we necessarily have $\mathsf{v}_\pm(\cdot, w) \not\equiv v(\cdot, w)$ for all $w > V_\pm$.

In the following two subsections, we propose two possible choices for the velocities $\mathsf{v}_\pm$ satisfying (5.1) and such that $\mathsf{v}_\pm(\cdot, w) \equiv v(\cdot, w)$ for all $w \le V_\pm$.

5.1. First option. In this subsection we consider problem (1.1), (1.3), (1.4) with

$$\mathsf{v}_\pm(\rho,w) \doteq \begin{cases} v(\rho,w) & \text{if } w \le V_\pm, \\ \frac{V_\pm}{w}\, v(\rho,w) & \text{if } w > V_\pm, \end{cases} \qquad \mathsf{f}_\pm(u) \doteq \rho \cdot \mathsf{v}_\pm(u), \tag{5.2}$$

where v is defined in $(2.3)_1$. Clearly $\mathsf{v}_\pm$ satisfy (5.1). Notice that both the fundamental diagram $\rho \mapsto f(\rho,w)$ and the "rescaled" fundamental diagrams $\rho \mapsto \mathsf{f}_\pm(\rho,w)$ attain their maximal values at $R(w) \doteq \mathcal{R}_w(0)$, therefore $\mathsf{R}_\pm$ given in (3.7) simply reduce to R defined in $(4.2)_1$, namely $\mathsf{R}_\pm(w) = R(w)$. In particular

$$f(R(w),w) = F(w) \ge \mathsf{f}_\pm(R(w),w) = \begin{cases} F(w) & \text{if } w \le V_\pm, \\ V_\pm \frac{F(w)}{w} & \text{if } w > V_\pm. \end{cases}$$

In the present case the maps $\mathsf{Q}_\pm \colon \Omega \times (0,+\infty) \to [0,+\infty)$ defined in (3.8) become

$$\mathsf{Q}_-(u_L) \doteq \begin{cases} \mathsf{f}_-(u_L) & \text{if } \rho_L \le R(w_L), \\ F(w_L) & \text{if } \rho_L > R(w_L) \text{ and } w \le V_-, \\ V_- \frac{F(w_L)}{w_L} & \text{if } \rho_L > R(w_L) \text{ and } w > V_-, \end{cases}$$

$$\mathsf{Q}_+(u_R,w_L) \doteq \begin{cases} F(w_L) & \text{if } \rho_*(u_R,w_L) \le R(w_L) \text{ and } w \le V_+, \\ V_+ \frac{F(w_L)}{w_L} & \text{if } \rho_*(u_R,w_L) \le R(w_L) \text{ and } w > V_+, \\ \mathsf{f}_+(u_*(u_R,w_L)) & \text{if } \rho_*(u_R,w_L) > R(w_L), \end{cases}$$

where $u_* \doteq (\rho_*, w_*)$ is defined in (3.5).

We run computer assisted numerical simulations of the FTL model (3.2), (5.2) and take $p(\rho) = \rho^\gamma$, $\gamma = 2$. In Figure 14–19 we plot $\mathtt{r}$ and $\mathtt{w}$ for some initial data of interest. We see a good agreement with the Riemann solver $\mathcal{RS}_{\mathfrak{R}_-,\mathfrak{R}_+}$ for (1.1), (1.3), (1.4), (5.2) given in Definition 3.1, at least in the cases under consideration.

We construct below $\mathcal{RS}_{\mathfrak{R}_-,\mathfrak{R}_+}[u_L,u_R]$ for the cases considered in Figure 14–19, with the aim to make Definition 3.1 more clear. For simplicity, below we use the notation introduced in (4.5).

(V1.a) For an initial datum as in Figure 14 we have

$$\left.\begin{array}{rcl} \rho_L > \mathsf{R}_-(w_L) & \Longrightarrow & \mathsf{Q}_-(u_L) = \mathsf{F}_-(w_L) \\ \rho_* > \mathsf{R}_+(w_L) & \Longrightarrow & \mathsf{Q}_+(u_R,w_L) = \mathsf{f}_+(u_*) \end{array}\right\} \Longrightarrow \mathsf{Q}(u_L,u_R) = \mathsf{f}_+(u_*).$$

$\mathcal{RS}_-[u_L,\hat{u}]$ is the 1-rarefaction $\mathcal{R}_1(u_L,\hat{u})$, and $\mathcal{RS}_+[\check{u},u_R]$ is the juxtaposition of the 1-shock $\mathcal{S}_1(\check{u},u_*)$ and the 2-contact discontinuity $\mathcal{C}_2(u_*,u_R)$. $\mathcal{S}_1(\check{u},u_*)$ is *stationary* and for this reason the ρ-component of $\mathcal{RS}_{\mathfrak{R}_-,\mathfrak{R}_+}[u_L,u_R]$ does not attain the value $\check{\rho}$.

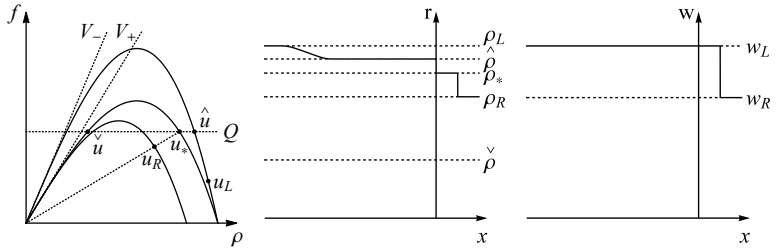

FIGURE 14. The approximate density (3.3), center, and approximate Lagrangian marker (3.4), right, corresponding to FTL model (3.2), (5.2) and the initial datum $(u_L, u_R) \in \Omega^2$, left. The solution obtained by applying the Riemann solver $\mathcal{RS}_{\mathfrak{R}_-,\mathfrak{R}_+}$ is described in **(V1.a)**.

(V1.b) For an initial datum as in Figure 15, we have

$$\left.\begin{array}{rcl} \rho_L > \mathsf{R}_-(w_L) & \Longrightarrow & \mathsf{Q}_-(u_L) = \mathsf{F}_-(w_L) \\ \rho_* < \mathsf{R}_+(w_L) & \Longrightarrow & \mathsf{Q}_+(u_R, w_L) = \mathsf{F}_+(w_L) \end{array}\right\} \Longrightarrow \mathsf{Q}(u_L, u_R) = \mathsf{F}_+(w_L).$$

$\mathcal{RS}_-[u_L, \hat{u}]$ is the 1-rarefaction $\mathcal{R}_1(u_L, \hat{u})$, and $\mathcal{RS}_+[\check{u}, u_R]$ is the juxtaposition of the 1-rarefaction $\mathcal{R}_1(\check{u}, u_*)$ and the 2-contact discontinuity $\mathcal{C}_2(u_*, u_R)$.

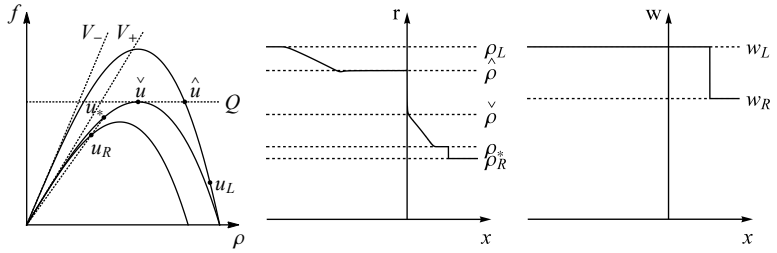

FIGURE 15. The approximate density (3.3), center, and approximate Lagrangian marker (3.4), right, corresponding to FTL model (3.2), (5.2) and the initial datum $(u_L, u_R) \in \Omega^2$, left. The solution obtained by applying the Riemann solver $\mathcal{RS}_{\mathfrak{R}_-,\mathfrak{R}_+}$ is described in **(V1.b)**.

(V1.c) For an initial datum as in Figure 16, we have

$$\left.\begin{array}{rcl} \rho_L > \mathsf{R}_-(w_L) & \Longrightarrow & \mathsf{Q}_-(u_L) = \mathsf{F}_-(w_L) \\ \rho_* > \mathsf{R}_+(w_L) & \Longrightarrow & \mathsf{Q}_+(u_R, w_L) = \mathsf{f}_+(u_*) \end{array}\right\} \Longrightarrow \mathsf{Q}(u_L, u_R) = \mathsf{F}_-(w_L).$$

$\mathcal{RS}_-[u_L, \hat{u}]$ is the 1-rarefaction $\mathcal{R}_1(u_L, \hat{u})$, and $\mathcal{RS}_+[\check{u}, u_R]$ is the juxtaposition of the 1-shock $\mathcal{S}_1(\check{u}, u_*)$ and the 2-contact discontinuity $\mathcal{C}_2(u_*, u_R)$.

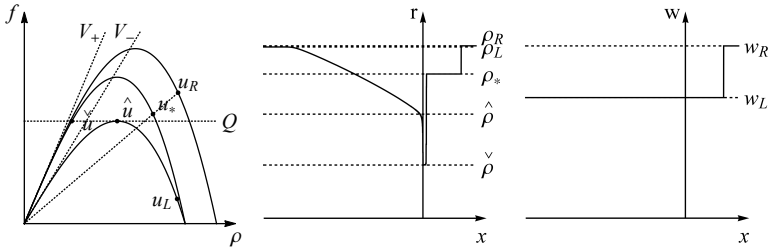

FIGURE 16. The approximate density (3.3), center, and approximate Lagrangian marker (3.4), right, corresponding to FTL model (3.2), (5.2) and the initial datum $(u_L, u_R) \in \Omega^2$, left. The solution obtained by applying the Riemann solver $\mathcal{RS}_{\mathfrak{R}_-,\mathfrak{R}_+}$ is described in **(V1.c)**.

(V1.d) For an initial datum as in Figure 17 the construction of $\mathcal{RS}_{\mathfrak{R}_-,\mathfrak{R}_+}[u_L, u_R]$ is analogous to that described in **(V1.c)**. Notice that differently from case **(V1.c)** here $w_R < w_L$.

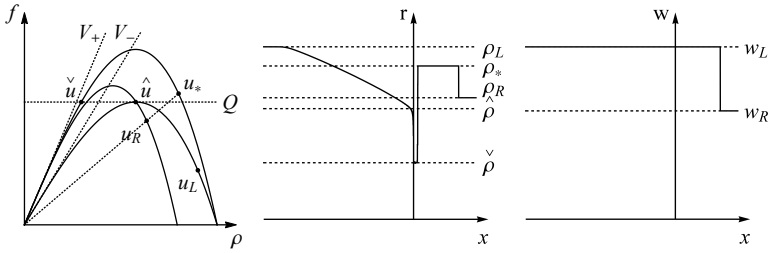

FIGURE 17. The approximate density (3.3), center, and approximate Lagrangian marker (3.4), right, corresponding to FTL model (3.2), (5.2) and the initial datum $(u_L, u_R) \in \Omega^2$, left. The solution obtained by applying the Riemann solver $\mathcal{RS}_{\mathfrak{R}_-,\mathfrak{R}_+}$ is described in **(V1.d)**.

(V1.e) For an initial datum as in Figure 18, we have

$$\left.\begin{array}{rl} \rho_L > \mathsf{R}_-(w_L) & \Longrightarrow \quad \mathsf{Q}_-(u_L) = \mathsf{F}_-(w_L) \\ \rho_* > \mathsf{R}_+(w_L) & \Longrightarrow \mathsf{Q}_+(u_R, w_L) = \mathsf{f}_+(u_*) \end{array}\right\} \Longrightarrow \mathsf{Q}(u_L, u_R) = \mathsf{f}_+(u_*).$$

$\mathcal{RS}_-[u_L, \hat{u}]$ is the 1-rarefaction $\mathcal{R}_1(u_L, \hat{u})$, and $\mathcal{RS}_+[\check{u}, u_R]$ is the juxtaposition of the 1-shock $\mathcal{S}_1(\check{u}, u_*)$ and the 2-contact discontinuity $\mathcal{C}_2(u_*, u_R)$. $\mathcal{S}_1(\check{u}, u_*)$ is *stationary* and for this reason the ρ-component of $\mathcal{RS}_{\mathfrak{R}_-,\mathfrak{R}_+}[u_L, u_R]$ does not attain the value $\check{\rho}$.

(V1.f) For an initial datum as in Figure 19, we have

$$\left.\begin{array}{rl} \rho_L < \mathsf{R}_-(w_L) & \Longrightarrow \quad \mathsf{Q}_-(u_L) = \mathsf{f}_-(u_L) \\ \rho_* < \mathsf{R}_+(w_L) & \Longrightarrow \mathsf{Q}_+(u_R, w_L) = \mathsf{F}_+(w_L) \end{array}\right\} \Longrightarrow \mathsf{Q}(u_L, u_R) = \mathsf{f}_-(u_L).$$

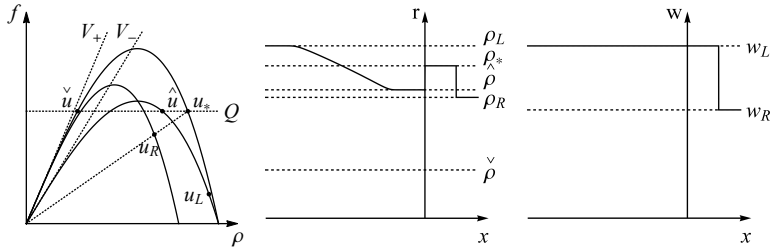

FIGURE 18. The approximate density (3.3), center, and approximate Lagrangian marker (3.4), right, corresponding to FTL model (3.2), (5.2) and the initial datum $(u_L, u_R) \in \Omega^2$, left. The solution obtained by applying the Riemann solver $\mathcal{RS}_{\mathfrak{R}_-,\mathfrak{R}_+}$ is described in **(V1.e)**.

$\mathcal{RS}_-[u_L, \hat{u}]$ is the 1-shock $\mathcal{S}_1(u_L, \hat{u})$, and $\mathcal{RS}_+[\check{u}, u_R]$ is the juxtaposition of the 1-rarefaction $\mathcal{R}_1(\check{u}, u_*)$ and the 2-contact discontinuity $\mathcal{C}_2(u_*, u_R)$. $\mathcal{S}_1(u_L, \hat{u})$ is *stationary* and for this reason the ρ-component of $\mathcal{RS}_{\mathfrak{R}_-,\mathfrak{R}_+}[u_L, u_R]$ does not attain the value $\hat{\rho}$. Notice that $\mathsf{v}_+(u_R) > w_L$ and for this reason $\rho_* = 0$.

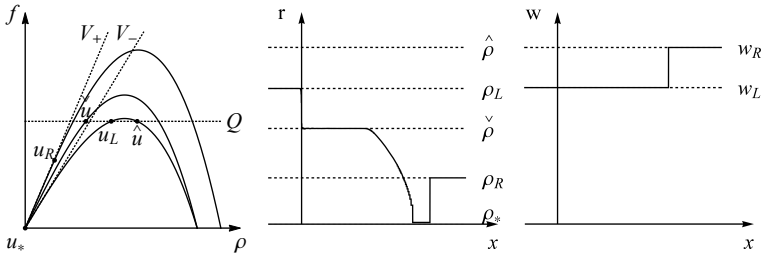

FIGURE 19. The approximate density (3.3), center, and approximate Lagrangian marker (3.4), right, corresponding to FTL model (3.2), (5.2) and the initial datum $(u_L, u_R) \in \Omega^2$, left. The solution obtained by applying the Riemann solver $\mathcal{RS}_{\mathfrak{R}_-,\mathfrak{R}_+}$ is described in **(V1.f)**.

5.2. Second option. In this subsection we consider problem (1.1), (1.3), (1.4) with

$$\mathsf{v}_\pm(u) \doteq \min\{V_\pm, v(u)\} = \begin{cases} V_\pm & \text{if } w > V_\pm \text{ and } \rho < p^{-1}(w - V_\pm), \\ v(u) & \text{otherwise,} \end{cases} \tag{5.3}$$

$$\mathsf{f}_\pm(u) \doteq \rho \cdot \mathsf{v}_\pm(u),$$

where v is defined in $(2.3)_1$. Observe that in the present case $\mathsf{R}_\pm(w)$ and $u_*(u_R, w_L)$ defined respectively in (3.5) and (3.7) become

$$\mathsf{R}_\pm(w) \doteq \max\{\mathcal{R}_w(0), p^{-1}([w - V_\pm]_+)\},$$
$$u_*(u_R, w_L) \doteq \big(p^{-1}([w_L - \mathsf{v}_+(u_R)]_+), w_L\big).$$

We run computer assisted numerical simulations of the FTL model (3.2), (5.3) with $p(\rho) = \rho^\gamma$, $\gamma = 2$. In Figures 20–25 we plot `r` and `w` for some initial data of interest. We see a good agreement with the Riemann solver $\mathcal{RS}_{\mathfrak{R}_-,\mathfrak{R}_+}$ for (1.1), (1.3), (1.4), (5.3) given in Definition 3.1, at least in the cases under consideration.

We construct below $\mathcal{RS}_{\mathfrak{R}_-,\mathfrak{R}_+}[u_L, u_R]$ for the cases considered in Figures 20–25, with the aim to make Definition 3.1 more clear. For simplicity, below we use the notation introduced in (4.5).

(V2.a) For an initial datum as in Figure 20 we have

$$\left.\begin{array}{rcl} \rho_L > \mathsf{R}_-(w_L) & \Longrightarrow & \mathsf{Q}_-(u_L) = \mathsf{F}_-(w_L) \\ \rho_* > \mathsf{R}_+(w_L) & \Longrightarrow & \mathsf{Q}_+(u_R, w_L) = \mathsf{f}_+(u_*) \end{array}\right\} \Longrightarrow \mathsf{Q}(u_L, u_R) = \mathsf{F}_-(w_L).$$

$\mathcal{RS}_-[u_L, \hat{u}]$ is the 1-rarefaction $\mathcal{R}_1(u_L, \hat{u})$, and $\mathcal{RS}_+[\check{u}, u_R]$ is the juxtaposition of the 1-shock $\mathcal{S}_1(\check{u}, u_*)$ and the 2-contact discontinuity $\mathcal{C}_2(u_*, u_R)$.

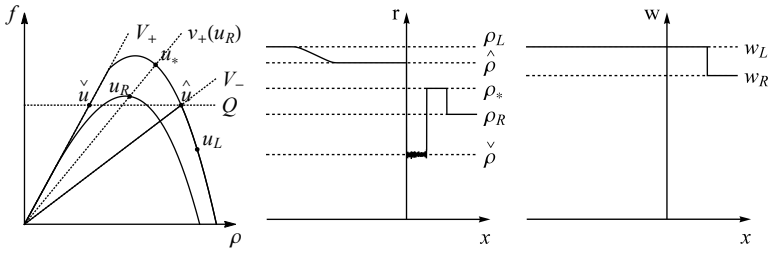

FIGURE 20. The approximate density (3.3), center, and approximate Lagrangian marker (3.4), right, corresponding to FTL model (3.2), (5.3) and initial datum $(u_L, u_R) \in \Omega^2$, left. The solution obtained by applying the Riemann solver $\mathcal{RS}_{\mathfrak{R}_-,\mathfrak{R}_+}$ is described in **(V2.a)**.

(V2.b) For an initial datum as in Figure 21, we have

$$\left.\begin{array}{rcl} \rho_L > \mathsf{R}_-(w_L) & \Longrightarrow & \mathsf{Q}_-(u_L) = \mathsf{F}_-(w_L) \\ \rho_* < \mathsf{R}_+(w_L) & \Longrightarrow & \mathsf{Q}_+(u_R, w_L) = \mathsf{F}_+(w_L) \end{array}\right\} \Longrightarrow \mathsf{Q}(u_L, u_R) = \mathsf{F}_-(w_L).$$

$\mathcal{RS}_-[u_L, \hat{u}]$ is the 1-rarefaction $\mathcal{R}_1(u_L, \hat{u})$, and $\mathcal{RS}_+[\check{u}, u_R]$ is the juxtaposition of the 1-rarefaction $\mathcal{R}_1(\check{u}, u_*)$ and the 2-contact discontinuity $\mathcal{C}_2(u_*, u_R)$.

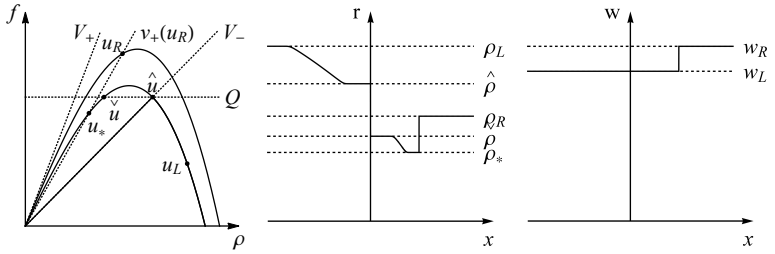

FIGURE 21. The approximate density (3.3), center, and approximate Lagrangian marker (3.4), right, corresponding to FTL model (3.2), (5.3) and initial datum $(u_L, u_R) \in \Omega^2$, left. The solution obtained by applying the Riemann solver $\mathcal{RS}_{\mathfrak{R}_-,\mathfrak{R}_+}$ is described in **(V2.b)**.

(V2.c) For an initial datum as in Figure 22, we have

$$\left.\begin{array}{rcl} \rho_L > \mathsf{R}_-(w_L) & \Longrightarrow & \mathsf{Q}_-(u_L) = \mathsf{F}_-(w_L) \\ \rho_* < \mathsf{R}_+(w_L) & \Longrightarrow & \mathsf{Q}_+(u_R, w_L) = \mathsf{F}_+(w_L) \end{array}\right\} \Longrightarrow \mathsf{Q}(u_L, u_R) = \mathsf{F}_-(w_L).$$

$\mathcal{RS}_-[u_L, \hat{u}]$ is the 1-rarefaction $\mathcal{R}_1(u_L, \hat{u})$, and $\mathcal{RS}_+[\check{u}, u_R]$ is the juxtaposition of the 1-shock $\mathcal{S}_1(\check{u}, u_*)$ and the 2-contact discontinuity $\mathcal{C}_2(u_*, u_R)$.

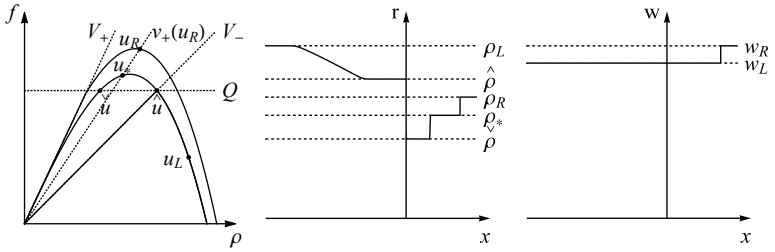

FIGURE 22. The approximate density (3.3), center, and approximate Lagrangian marker (3.4), right, corresponding to FTL model (3.2), (5.3) and initial datum $(u_L, u_R) \in \Omega^2$, left. The solution obtained by applying the Riemann solver $\mathcal{RS}_{\mathfrak{R}_-,\mathfrak{R}_+}$ is described in **(V2.c)**.

(V2.d) For an initial datum as in Figure 23, we have

$$\left.\begin{array}{rcl} \rho_L > \mathsf{R}_-(w_L) & \Longrightarrow & \mathsf{Q}_-(u_L) = \mathsf{F}_-(w_L) \\ \rho_* > \mathsf{R}_+(w_L) & \Longrightarrow & \mathsf{Q}_+(u_R, w_L) = \mathsf{f}_+(u_*) \end{array}\right\} \Longrightarrow \mathsf{Q}(u_L, u_R) = \mathsf{f}_+(u_*).$$

$\mathcal{RS}_-[u_L, \hat{u}]$ is the 1-rarefaction $\mathcal{R}_1(u_L, \hat{u})$, and $\mathcal{RS}_+[\check{u}, u_R]$ is the juxtaposition of the 1-shock $\mathcal{S}_1(\check{u}, u_*)$ and the 2-contact discontinuity $\mathcal{C}_2(u_*, u_R)$. $\mathcal{S}_1(\check{u}, u_*)$ is *stationary* and for this reason the

ρ-component of $\mathcal{RS}_{\mathfrak{R}_-,\mathfrak{R}_+}[u_L, u_R]$ does not attain the value $\check{\rho}$. Notice that $u_* = \hat{u}$.

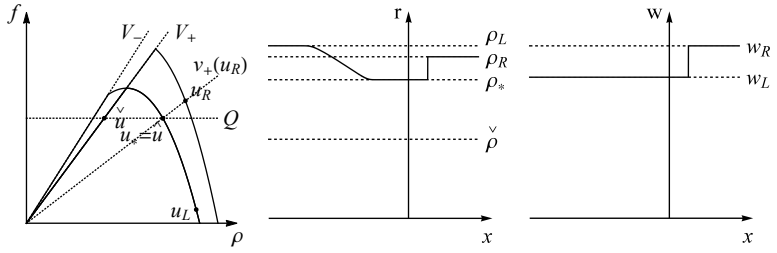

FIGURE 23. The approximate density (3.3), center, and approximate Lagrangian marker (3.4), right, corresponding to FTL model (3.2), (5.3) and initial datum $(u_L, u_R) \in \Omega^2$, left. The solution obtained by applying the Riemann solver $\mathcal{RS}_{\mathfrak{R}_-,\mathfrak{R}_+}$ is described in **(V2.d)**.

(V2.e) For an initial datum as in Figure 24, we have

$$\left.\begin{array}{ll} \rho_L < \mathsf{R}_-(w_L) & \Longrightarrow \quad \mathsf{Q}_-(u_L) = \mathsf{f}_-(u_L) \\ \rho_* > \mathsf{R}_+(w_L) & \Longrightarrow \mathsf{Q}_+(u_R, w_L) = \mathsf{f}_+(u_*) \end{array}\right\} \Longrightarrow \mathsf{Q}(u_L, u_R) = \mathsf{f}_+(u_*).$$

$\mathcal{RS}_-[u_L, \hat{u}]$ is the 1-shock $\mathcal{S}_1(u_L, \hat{u})$, and $\mathcal{RS}_+[\check{u}, u_R]$ is the juxtaposition of the 1-shock $\mathcal{S}_1(\check{u}, u_*)$ and the 2-contact discontinuity $\mathcal{C}_2(u_*, u_R)$. $\mathcal{S}_1(\check{u}, u_*)$ is *stationary* and for this reason the ρ-component of $\mathcal{RS}_{\mathfrak{R}_-,\mathfrak{R}_+}[u_L, u_R]$ does not attain the value $\check{\rho}$. Notice that $u_* = \hat{u}$.

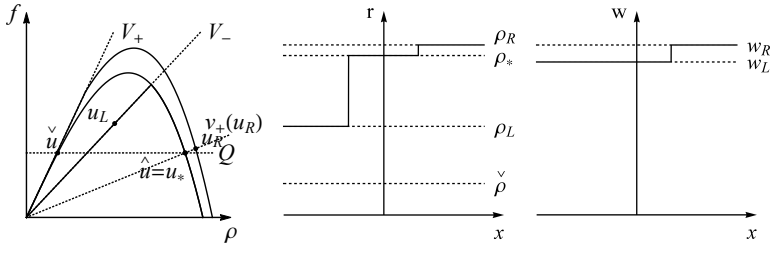

FIGURE 24. The approximate density (3.3), center, and approximate Lagrangian marker (3.4), right, corresponding to FTL model (3.2), (5.3) and initial datum $(u_L, u_R) \in \Omega^2$, left. The solution obtained by applying the Riemann solver $\mathcal{RS}_{\mathfrak{R}_-,\mathfrak{R}_+}$ is described in **(V2.e)**.

(V2.f) For an initial datum as in Figure 25, we have

$$\left.\begin{array}{ll} \rho_L < \mathsf{R}_-(w_L) & \Longrightarrow \quad \mathsf{Q}_-(u_L) = \mathsf{f}_-(u_L) \\ \rho_* > \mathsf{R}_+(w_L) & \Longrightarrow \mathsf{Q}_+(u_R, w_L) = \mathsf{f}_+(u_*) \end{array}\right\} \Longrightarrow \mathsf{Q}(u_L, u_R) = \mathsf{f}_-(u_L).$$

$\mathcal{RS}_-[u_L, \hat{u}]$ is the 1-shock $\mathcal{S}_1(u_L, \hat{u})$, and $\mathcal{RS}_+[\check{u}, u_R]$ is the juxtaposition of the 1-shock $\mathcal{S}_1(\check{u}, u_*)$ and the 2-contact discontinuity $\mathcal{C}_2(u_*, u_R)$. $\mathcal{S}_1(u_L, \hat{u})$ is *stationary* and for this reason the ρ-component of $\mathcal{RS}_{\mathfrak{R}_-,\mathfrak{R}_+}[u_L, u_R]$ does not attain the value $\hat{\rho}$.

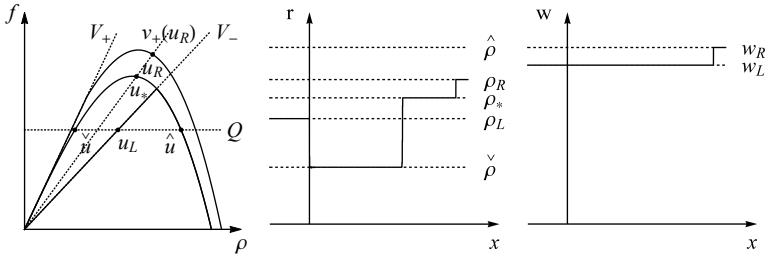

FIGURE 25. The approximate density (3.3), center, and approximate Lagrangian marker (3.4), right, corresponding to FTL model (3.2), (5.3) and initial datum $(u_L, u_R) \in \Omega^2$, left. The solution obtained by applying the Riemann solver $\mathcal{RS}_{\mathfrak{R}_-,\mathfrak{R}_+}$ is described in **(V2.f)**.

6. ARZ model for two roads with different capacities and speed limits

In this section we consider two roads $\mathfrak{R}_- \doteq (-\infty, 0)$ and $\mathfrak{R}_+ \doteq [0, +\infty)$ with capacities $F_- > 0$ and $F_+ > 0$, respectively, and with speed limits $V_- > 0$ and $V_+ > 0$, respectively. Then the evolution of traffic along $\mathbb{R}$ can be described by (1.1), (1.3), (1.4) with $\mathsf{f}_\pm \colon \Omega \to [0, +\infty)$ satisfying (4.1) and $\mathsf{v}_\pm \colon \Omega \to [0, +\infty)$ satisfying (5.1).

6.1. First option. In analogy with Subsections 4.1 and 5.1, here we take

$$\mathsf{v}_\pm(\rho, w) \doteq \min\left\{ \frac{\min\{F_\pm, F(w)\}}{F(w)}, \frac{\min\{V_\pm, w\}}{w} \right\} v(\rho, w)$$

$$= \begin{cases} v(\rho, w) & \text{if } w \le W_\pm \text{ and } w \le V_\pm, \\ \frac{F_\pm}{F(w)}\, v(\rho, w) & \text{if } w > W_\pm \text{ and } w \le V_\pm, \\ \frac{V_\pm}{w}\, v(\rho, w) & \text{if } w \le W_\pm \text{ and } w > V_\pm, \\ \min\left\{ \frac{F_\pm}{F(w)}, \frac{V_\pm}{w} \right\} v(\rho, w) & \text{if } w > W_\pm \text{ and } w > V_\pm, \end{cases} \tag{6.1}$$

where F and $W_\pm$ are defined $(4.2)_2$ and $(4.2)_3$, respectively.

We run computer assisted numerical simulations of the FTL model (3.2), (6.1) with $p(\rho) = \rho^\gamma$, $\gamma = 2$. In Figures 26–31 we plot $\mathtt{r}$ and $\mathtt{w}$ for some initial data of interest. We see a good agreement with the Riemann solver $\mathcal{RS}_{\mathfrak{R}_-,\mathfrak{R}_+}$ for (1.1), (1.3), (1.4), (6.1) given in Definition 3.1, at least in the cases under consideration.

We construct below $\mathcal{RS}_{\mathfrak{R}_-,\mathfrak{R}_+}[u_L,u_R]$ for the cases considered in Figures 26–31, with the aim to make Definition 3.1 more clear. For simplicity, below we use the notation introduced in (4.5).

(FV1.a) For an initial datum as in Figure 26, we have

$$\left.\begin{array}{rl} \rho_L > \mathsf{R}_-(w_L) & \Longrightarrow \quad \mathsf{Q}_-(u_L) = \mathsf{F}_-(w_L) \\ \rho_* > \mathsf{R}_+(w_L) & \Longrightarrow \mathsf{Q}_+(u_R,w_L) = \mathsf{f}_+(u_*) \end{array}\right\} \Longrightarrow \mathsf{Q}(u_L,u_R) = \mathsf{f}_+(u_*).$$

$\mathcal{RS}_-[u_L,\hat{u}]$ is the 1-rarefaction $\mathcal{R}_1(u_L,\hat{u})$, and $\mathcal{RS}_+[\check{u},u_R]$ is the juxtaposition of the 1-shock $\mathcal{S}_1(\check{u},u_*)$ and the 2-contact discontinuity $\mathcal{C}_2(u_*,u_R)$. $\mathcal{S}_1(\check{u},u_*)$ is a *stationary* shock and for this reason the ρ-component of $\mathcal{RS}_{\mathfrak{R}_-,\mathfrak{R}_+}[u_L,u_R]$ does not attain the value $\check{\rho}$.

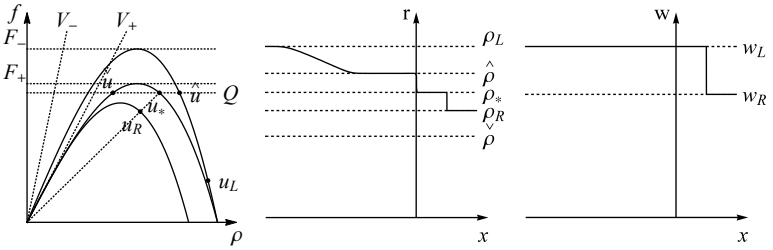

FIGURE 26. The approximate density (3.3), center, and approximate Lagrangian marker (3.4), right, corresponding to FTL model (3.2), (6.1) and initial datum $(u_L,u_R) \in \Omega^2$, left. The solution obtained by applying the Riemann solver $\mathcal{RS}_{\mathfrak{R}_-,\mathfrak{R}_+}$ is described in **(FV1.a)**.

(FV1.b) For an initial datum as in Figure 27, we have

$$\left.\begin{array}{rl} \rho_L > \mathsf{R}_-(w_L) & \Longrightarrow \quad \mathsf{Q}_-(u_L) = \mathsf{F}_-(w_L) \\ \rho_* < \mathsf{R}_+(w_L) & \Longrightarrow \mathsf{Q}_+(u_R,w_L) = \mathsf{F}_+(w_L) \end{array}\right\} \Longrightarrow \mathsf{Q}(u_L,u_R) = \mathsf{F}_+(w_L).$$

$\mathcal{RS}_-[u_L,\hat{u}]$ is the 1-rarefaction $\mathcal{R}_1(u_L,\hat{u})$, and $\mathcal{RS}_+[\check{u},u_R]$ is the juxtaposition of the 1-rarefaction $\mathcal{R}_1(\check{u},u_*)$ and the 2-contact discontinuity $\mathcal{C}_2(u_*,u_R)$.

(FV1.c) For an initial datum as in Figure 28, we have

$$\left.\begin{array}{rl} \rho_L < \mathsf{R}_-(w_L) & \Longrightarrow \quad \mathsf{Q}_-(u_L) = \mathsf{f}_-(u_L) \\ \rho_* > \mathsf{R}_+(w_L) & \Longrightarrow \mathsf{Q}_+(u_R,w_L) = \mathsf{f}_+(w_L) \end{array}\right\} \Longrightarrow \mathsf{Q}(u_L,u_R) = \mathsf{f}_-(u_L).$$

$\mathcal{RS}_-[u_L,\hat{u}]$ is the 1-shock $\mathcal{S}_1(u_L,\hat{u})$, and $\mathcal{RS}_+[\check{u},u_R]$ is the juxtaposition of the 1-shock $\mathcal{S}_1(\check{u},u_*)$ and the 2-contact discontinuity $\mathcal{C}_2(u_*,u_R)$. $\mathcal{S}_1(u_L,\hat{u})$ is a *stationary* shock and for this reason the ρ-component of $\mathcal{RS}_{\mathfrak{R}_-,\mathfrak{R}_+}[u_L,u_R]$ does not attain the value $\hat{\rho}$.

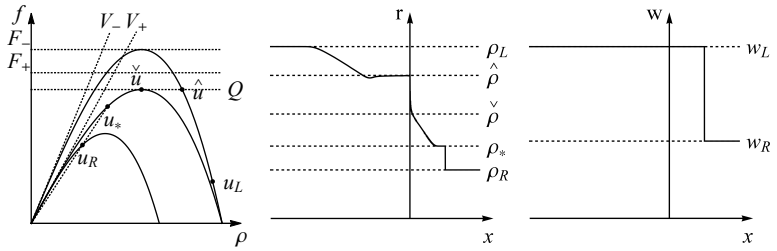

FIGURE 27. The approximate density (3.3), center, and approximate Lagrangian marker (3.4), right, corresponding to FTL model (3.2), (6.1) and initial datum $(u_L, u_R) \in \Omega^2$, left. The solution obtained by applying the Riemann solver $\mathcal{RS}_{\mathfrak{R}_-,\mathfrak{R}_+}$ is described in **(FV1.b)**.

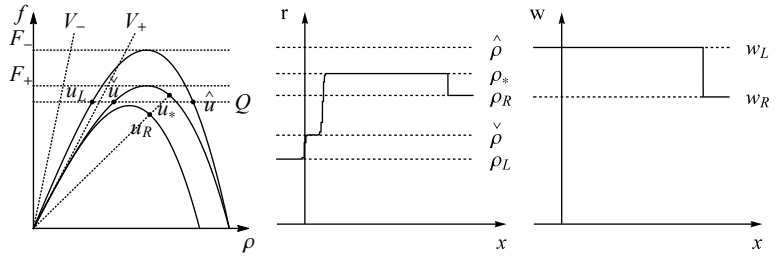

FIGURE 28. The approximate density (3.3), center, and approximate Lagrangian marker (3.4), right, corresponding to FTL model (3.2), (6.1) and initial datum $(u_L, u_R) \in \Omega^2$, left. The solution obtained by applying the Riemann solver $\mathcal{RS}_{\mathfrak{R}_-,\mathfrak{R}_+}$ is described in **(FV1.c)**.

(FV1.d) For an initial datum as in Figure 29, we have

$$\left.\begin{array}{rl} \rho_L < \mathsf{R}_-(w_L) & \Longrightarrow \quad \mathsf{Q}_-(u_L) = \mathsf{f}_-(u_L) \\ \rho_* < \mathsf{R}_+(w_L) & \Longrightarrow \mathsf{Q}_+(u_R, w_L) = \mathsf{F}_+(w_L) \end{array}\right\} \Longrightarrow \mathsf{Q}(u_L, u_R) = \mathsf{f}_-(u_L).$$

$\mathcal{RS}_-[u_L, \hat{u}]$ is the 1-shock $\mathcal{S}_1(u_L, \hat{u})$, and $\mathcal{RS}_+[\check{u}, u_R]$ is the juxtaposition of the 1-shock $\mathcal{S}_1(\check{u}, u_*)$ and the 2-contact discontinuity $\mathcal{C}_2(u_*, u_R)$. $\mathcal{S}_1(u_L, \hat{u})$ is a *stationary* shock and for this reason the ρ-component of $\mathcal{RS}_{\mathfrak{R}_-,\mathfrak{R}_+}[u_L, u_R]$ does not attain the value $\hat{\rho}$.

(FV1.e) For an initial datum as in Figure 30, we have

$$\left.\begin{array}{rl} \rho_L > \mathsf{R}_-(w_L) & \Longrightarrow \quad \mathsf{Q}_-(u_L) = \mathsf{F}_-(u_L) = F_- \\ \rho_* < \mathsf{R}_+(w_L) & \Longrightarrow \mathsf{Q}_+(u_R, w_L) = \mathsf{F}_+(w_L) = F_+ \end{array}\right\} \Longrightarrow \mathsf{Q}(u_L, u_R) = F_+.$$

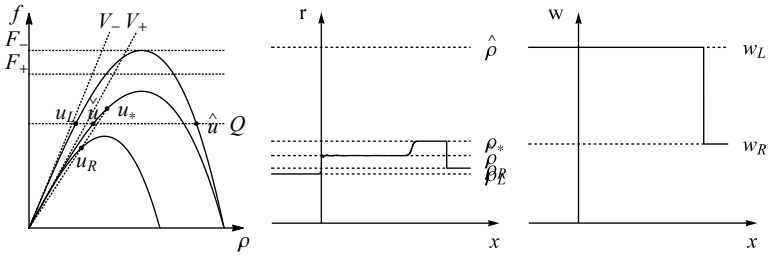

FIGURE 29. The approximate density (3.3), center, and approximate Lagrangian marker (3.4), right, corresponding to FTL model (3.2), (6.1) and initial datum $(u_L, u_R) \in \Omega^2$, left. The solution obtained by applying the Riemann solver $\mathcal{RS}_{\mathfrak{R}_-,\mathfrak{R}_+}$ is described in **(FV1.d)**.

$\mathcal{RS}_-[u_L, \hat{u}]$ is the 1-rarefaction $\mathcal{R}_1(u_L, \hat{u})$, and $\mathcal{RS}_+[\check{u}, u_R]$ is the juxtaposition of the 1-rarefaction $\mathcal{R}_1(\check{u}, u_*)$ and the 2-contact discontinuity $\mathcal{C}_2(u_*, u_R)$.

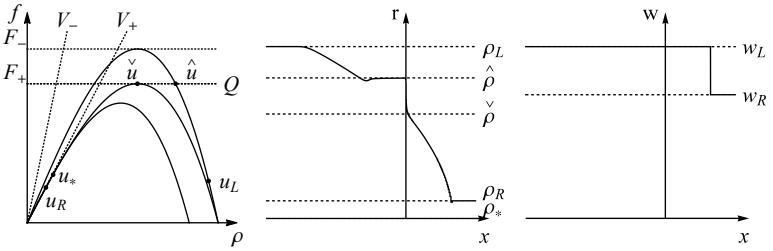

FIGURE 30. The approximate density (3.3), center, and approximate Lagrangian marker (3.4), right, corresponding to FTL model (3.2), (6.1) and initial datum $(u_L, u_R) \in \Omega^2$, left. The solution obtained by applying the Riemann solver $\mathcal{RS}_{\mathfrak{R}_-,\mathfrak{R}_+}$ is described in **(FV1.e)**.

(FV1.f) For an initial datum as in Figure 31, we have

$$\left.\begin{array}{rcl} \rho_L > \mathsf{R}_-(w_L) & \Longrightarrow & \mathsf{Q}_-(u_L) = \mathsf{F}_-(u_L) = F_- \\ \rho_* < \mathsf{R}_+(w_L) & \Longrightarrow & \mathsf{Q}_+(u_R, w_L) = \mathsf{F}_+(w_L) = F_+ \end{array}\right\} \Longrightarrow \mathsf{Q}(u_L, u_R) = F_-.$$

$\mathcal{RS}_-[u_L, \hat{u}]$ is the 1-rarefaction $\mathcal{R}_1(u_L, \hat{u})$, and $\mathcal{RS}_+[\check{u}, u_R]$ is the juxtaposition of the 1-rarefaction $\mathcal{R}_1(\check{u}, u_*)$ and the 2-contact discontinuity $\mathcal{C}_2(u_*, u_R)$. Notice that $\mathsf{v}_+(u_R) > w_L$ and for this reason $\rho_* = 0$.

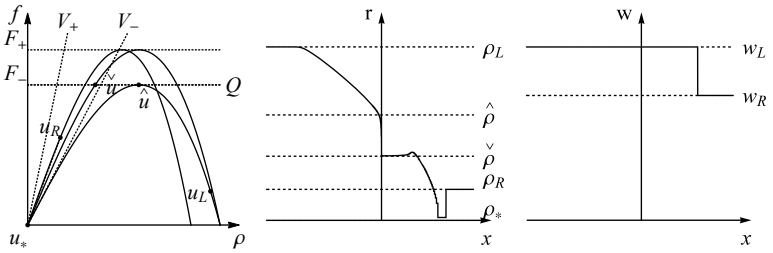

FIGURE 31. The approximate density (3.3), center, and approximate Lagrangian marker (3.4), right, corresponding to FTL model (3.2), (6.1) and initial datum $(u_L, u_R) \in \Omega^2$, left. The solution obtained by applying the Riemann solver $\mathcal{RS}_{\mathfrak{R}_-,\mathfrak{R}_+}$ is described in **(FV1.f)**.

6.2. Second option. In analogy with Subsections 4.2 and 5.2, here we take

$$
\mathsf{v}_\pm(\rho, w) \doteq \begin{cases} \min\{F_\pm/\rho, V_\pm\} & \text{if } w > \max\{W_\pm, V_\pm\}, f(\rho, w) > F_\pm \\ & \text{and } \rho < p^{-1}(w - V_\pm), \\ F_\pm/\rho & \text{if } w > W_\pm,\ f(\rho, w) > F_\pm \\ & \text{and } w \le V_\pm, \\ F_\pm/\rho & \text{if } w > W_\pm, f(\rho, w) > F_\pm \\ & \text{and } \rho \ge p^{-1}(w - V_\pm), \\ V_\pm & \text{if } w > V_\pm,\ \rho < p^{-1}(w - V_\pm) \\ & \text{and } w \le W_\pm, \\ V_\pm & \text{if } w > V_\pm, \rho < p^{-1}(w - V_\pm) \\ & \text{and } f(\rho, w) \le F_\pm, \\ v(\rho, w) & \text{otherwise,} \end{cases} \tag{6.2}
$$

where F and $W_\pm$ are defined $(4.2)_2$ and $(4.2)_3$, respectively.

We run computer assisted numerical simulations of the FTL model (3.2), (6.2) with $p(\rho) = \rho^\gamma$, $\gamma = 2$. In Figures 32–37 we plot $\mathtt{r}$ and $\mathtt{w}$ for some initial data of interest. We see a good agreement with the Riemann solver $\mathcal{RS}_{\mathfrak{R}_-,\mathfrak{R}_+}$ for (1.1), (1.3), (1.4), (6.2) given in Definition 3.1, at least in the cases under consideration.

We construct below $\mathcal{RS}_{\mathfrak{R}_-,\mathfrak{R}_+}[u_L, u_R]$ for the cases considered in Figures 32–37, with the aim to make Definition 3.1 more clear. For simplicity, below we use the notation introduced in (4.5).

(FV2.a) For an initial datum as in Figure 32, we have

$$
\left.\begin{array}{l} \rho_L > \mathsf{R}_-(w_L) \implies \mathsf{Q}_-(u_L) = \mathsf{F}_-(w_L) \\ \rho_* > \mathsf{R}_+(w_L) \implies \mathsf{Q}_+(u_R, w_L) = \mathsf{f}_+(u_*) \end{array}\right\} \implies \mathsf{Q}(u_L, u_R) = \mathsf{f}_+(u_*).
$$

$\mathcal{RS}_-[u_L, \hat{u}]$ is the 1-shock $\mathcal{S}_1(u_L, \hat{u})$, and $\mathcal{RS}_+[\check{u}, u_R]$ is the juxtaposition of the 1-shock $\mathcal{S}_1(\check{u}, u_*)$ and the 2-contact discontinuity $\mathcal{C}_2(u_*, u_R)$. $\mathcal{S}_1(\check{u}, u_*)$ is *stationary* and for this reason the ρ-component of $\mathcal{RS}_{\mathfrak{R}_-,\mathfrak{R}_+}[u_L, u_R]$ does not attain the value $\check{\rho}$.

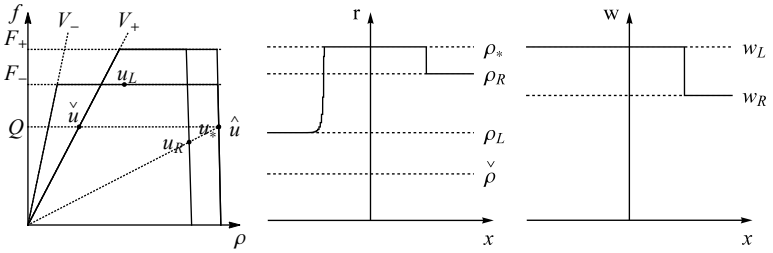

FIGURE 32. The approximate density (3.3), center, and approximate Lagrangian marker (3.4), right, corresponding to FTL model (3.2), (6.2) and initial datum $(u_L, u_R) \in \Omega^2$, left. The solution obtained by applying the Riemann solver $\mathcal{RS}_{\mathfrak{R}_-,\mathfrak{R}_+}$ is described in **(FV2.a)**.

(FV2.b) For an initial datum as in Figure 33, we see that the construction of the solution is analogous to that described in **(FV2.a)**. Notice that differently from case **(FV2.a)**, here $F_+ < F_-$.

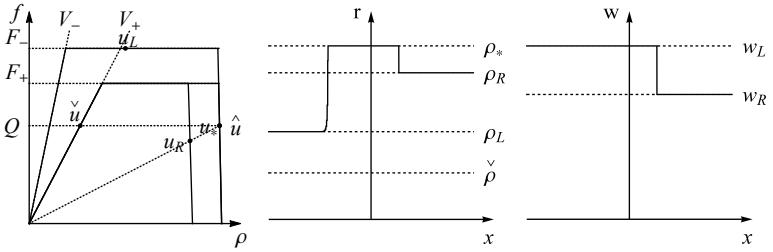

FIGURE 33. The approximate density (3.3), center, and approximate Lagrangian marker (3.4), right, corresponding to FTL model (3.2), (6.2) and initial datum $(u_L, u_R) \in \Omega^2$, left. The solution obtained by applying the Riemann solver $\mathcal{RS}_{\mathfrak{R}_-,\mathfrak{R}_+}$ is described in **(FV2.b)**.

(FV2.c) For an initial datum as in Figure 34, we see that the construction of the solution is analogous to that described in **(FV2.a)**. Notice that differently from case **(FV2.a)**, here $V_- < V_+$.

(FV2.d) For an initial datum as in Figure 35, we have

$$\left.\begin{array}{rl} \rho_L > \mathsf{R}_-(w_L) & \Longrightarrow \quad \mathsf{Q}_-(u_L) = \mathsf{F}_-(w_L) = F_- \\ \rho_* < \mathsf{R}_+(w_L) & \Longrightarrow \mathsf{Q}_+(u_R, w_L) = \mathsf{F}_+(w_L) = F_+ \end{array}\right\} \Longrightarrow \mathsf{Q}(u_L, u_R) = \mathsf{F}_-.$$

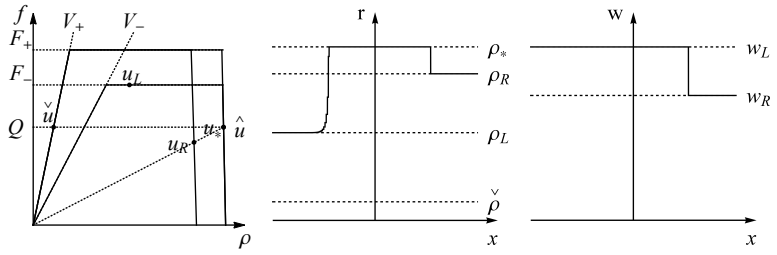

FIGURE 34. The approximate density (3.3), center, and approximate Lagrangian marker (3.4), right, corresponding to FTL model (3.2), (6.2) and initial datum $(u_L, u_R) \in \Omega^2$, left. The solution obtained by applying the Riemann solver $\mathcal{RS}_{\mathfrak{R}_-,\mathfrak{R}_+}$ is described in **(FV2.c)**.

$\mathcal{RS}_-[u_L, \hat{u}]$ is the 1-contact discontinuity $\mathcal{C}_1(u_L, \hat{u})$, and $\mathcal{RS}_+[\check{u}, u_R]$ is the juxtaposition of the 1-shock $\mathcal{S}_1(\check{u}, u_*)$ and the 2-contact discontinuity $\mathcal{C}_2(u_*, u_R)$. $\mathcal{C}_1(u_L, \hat{u})$ is *stationary* and for this reason the ρ-component of $\mathcal{RS}_{\mathfrak{R}_-,\mathfrak{R}_+}[u_L, u_R]$ does not attain the value $\hat{\rho}$.

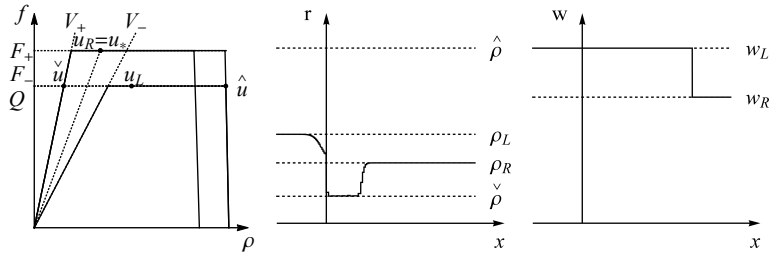

FIGURE 35. The approximate density (3.3), center, and approximate Lagrangian marker (3.4), right, corresponding to FTL model (3.2), (6.2) and initial datum $(u_L, u_R) \in \Omega^2$, left. The solution obtained by applying the Riemann solver $\mathcal{RS}_{\mathfrak{R}_-,\mathfrak{R}_+}$ is described in **(FV2.d)**.

(FV2.e) For an initial datum as in Figure 36, we have

$$\left.\begin{array}{rcl} \rho_L < \mathsf{R}_-(w_L) & \Longrightarrow & \mathsf{Q}_-(u_L) = \mathsf{f}_-(u_L) \\ \rho_* < \mathsf{R}_+(w_L) & \Longrightarrow & \mathsf{Q}_+(u_R, w_L) = \mathsf{F}_+(w_L) \end{array}\right\} \Longrightarrow \mathsf{Q}(u_L, u_R) = \mathsf{f}_-(u_L).$$

$\mathcal{RS}_-[u_L, \hat{u}]$ is the 1-shock $\mathcal{S}_1(u_L, \hat{u})$, and $\mathcal{RS}_+[\check{u}, u_R]$ is the juxtaposition of the 1-shock $\mathcal{S}_1(\check{u}, u_*)$ and the 2-contact discontinuity $\mathcal{C}_2(u_*, u_R)$. $\mathcal{S}_1(u_L, \hat{u})$ is *stationary* and for this reason the ρ-component of $\mathcal{RS}_{\mathfrak{R}_-,\mathfrak{R}_+}[u_L, u_R]$ does not attain the value $\hat{\rho}$. Notice that $\rho_* = \rho_R$ but $w_* \neq w_R$.

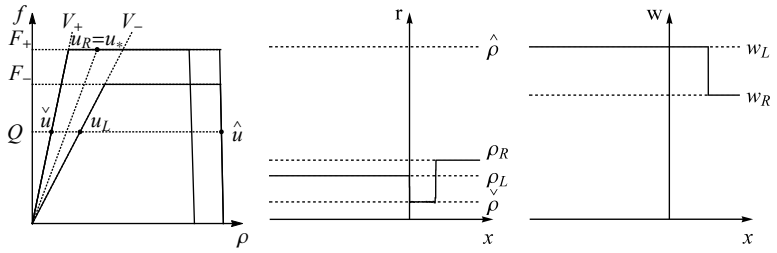

FIGURE 36. The approximate density (3.3), center, and approximate Lagrangian marker (3.4), right, corresponding to FTL model (3.2), (6.2) and initial datum $(u_L, u_R) \in \Omega^2$, left. The solution obtained by applying the Riemann solver $\mathcal{RS}_{\mathfrak{R}_-,\mathfrak{R}_+}$ is described in **(FV2.e)**.

(FV2.f) For an initial datum as in Figure 37, we have

$$\left.\begin{array}{ll} \rho_L > \mathsf{R}_-(w_L) & \Longrightarrow \quad \mathsf{Q}_-(u_L) = \mathsf{F}_-(w_L) = F_- \\ \rho_* < \mathsf{R}_+(w_L) & \Longrightarrow \mathsf{Q}_+(u_R, w_L) = \mathsf{F}_+(w_L) = F_+ \end{array}\right\} \Longrightarrow \mathsf{Q}(u_L, u_R) = F_-.$$

$\mathcal{RS}_-[u_L, \hat{u}]$ is the 1-rarefaction $\mathcal{R}_1(u_L, \hat{u})$, and $\mathcal{RS}_+[\check{u}, u_R]$ is the 2-contact discontinuity $\mathcal{C}_2(\check{u}, u_R)$.

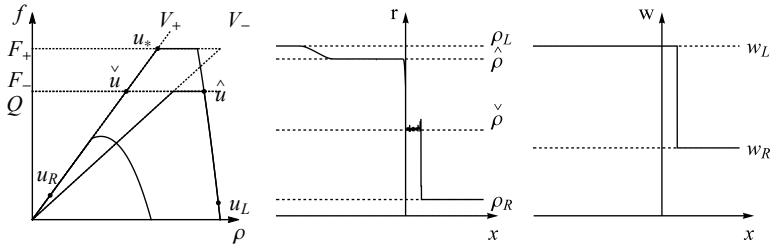

FIGURE 37. The approximate density (3.3), center, and approximate Lagrangian marker (3.4), right, corresponding to FTL model (3.2), (6.2) and initial datum $(u_L, u_R) \in \Omega^2$, left. The solution obtained by applying the Riemann solver $\mathcal{RS}_{\mathfrak{R}_-,\mathfrak{R}_+}$ is described in **(FV2.f)**.

7. ARZ model with point constraint

In this section we briefly show a possible application of the previous results. Consider a road with a pointwise bottleneck at $x = 0$ characterized by either maximal capacity F_0 or speed limit V_0. Beside the ARZ model (2.1) we enforce in the former case the condition

$$f(u)(t, 0^{\pm}) \le F_0, \quad t > 0 \tag{7.1}$$

and in the latter case the condition

$$v(t,0^+) \le V_0, \quad t>0. \tag{7.2}$$

As in [18], we introduce an interval $I_\varepsilon \doteq (-\varepsilon,\varepsilon)$, $\varepsilon>0$, and enforce therein in the former case the condition

$$f(u(t,x))\cdot \mathbb{1}_{I_\varepsilon}(x) \le F_0 \tag{7.3}$$

and in the latter case the condition

$$v(u(t,x))\cdot \mathbb{1}_{I_\varepsilon}(x) \le V_0. \tag{7.4}$$

Then we envisage two approaches to construct the approximate solutions $u^\varepsilon_{F_0}$ and $u^\varepsilon_{V_0}$ to the approximate constrained Riemann problem (2.1), (7.3), (1.5) and (2.1), (7.4), (1.5), respectively: either one can apply a wave-front tracking method analogous to that proposed in [9] and based on the Riemann solvers already obtained in Sections 4 and 5, or one can introduce microscopic FTL models analogous to those obtained in Sections 4 and 5. In both cases, the next step is to let ε go to 0^+ and define the limits of $u^\varepsilon_{F_0}$ and $u^\varepsilon_{V_0}$ as the solutions to the constrained Riemann problems (2.1), (2.2), (7.1), (1.5) and (2.1), (2.2), (7.2), (1.5), respectively.

The first approach is quite standard. We give some more details on the second approach. If we are dealing with constraint (7.3), then in analogy to Subsections 4.1 and 4.2, we can consider the FTL model (3.1), (3.2) with either

$$\mathsf{v}(\rho,w,x) \doteq \begin{cases} \frac{F_0}{F(w)}\, v(\rho,w) & \text{if } x\in I_\varepsilon \text{ and } w>W,\\ v(\rho,w) & \text{otherwise,}\end{cases}$$
$$\mathsf{f}(u) \doteq \rho\cdot \mathsf{v}(u),$$

or

$$\mathsf{v}(\rho,w,x) \doteq \begin{cases} \frac{F_0}{\rho} & \text{if } x\in I_\varepsilon,\ w>W \text{ and } f(\rho,w)>F_0,\\ v(\rho,w) & \text{otherwise,}\end{cases}$$
$$\mathsf{f}(u) \doteq \rho\cdot \mathsf{v}(u),$$

where v is defined in $(2.3)_1$ and $W \doteq F^{-1}(F_0)$, where F is defined in $(4.2)_2$. If we are dealing with constraint (7.4), then in analogy to Subsections 5.1 and 5.2, we can consider the FTL model (3.1), (3.2) with either

$$\mathsf{v}(\rho,w,x) \doteq \begin{cases} \frac{V_0}{w}\, v(\rho,w) & \text{if } x\in I_\varepsilon \text{ and } w>V_0,\\ v(\rho,w) & \text{otherwise,}\end{cases}$$
$$\mathsf{f}(u) \doteq \rho\cdot \mathsf{v}(u),$$

or

$$\mathsf{v}(\rho,w,x) \doteq \begin{cases} V_0 & \text{if } x\in I_\varepsilon,\ w>V_0 \text{ and } v(\rho,w)>V_0,\\ v(\rho,w) & \text{otherwise,}\end{cases}$$
$$\mathsf{f}(u) \doteq \rho\cdot \mathsf{v}(u).$$

We stress that we are focused on the waves created at $x = \pm\varepsilon$ and $x = 0$, as well as on the interactions among these waves. On the contrary, the remaining waves created at $x = \pm\delta$ are not of interest, as well as their interactions with the other waves. For this reason $\delta > 0$ has to be chosen big enough and only the solution in a vicinity of I_ε has to be studied.

Again, numerical simulations for carefully identified sets of data can select physically reasonable Riemann solvers. However, this is not the aim of the present paper and is deferred to future works.

Acknowledgments. The author thanks Boris Andreianov for some discussions on the subject of the paper. The author is member of GNAMPA. He acknowledges the support of the National Science Centre, Poland, Project "Mathematics of multi-scale approaches in life and social sciences" No. 2017/25/B/ST1/00051, of the INdAM-GNAMPA Project 2019 "Equazioni alle derivate parziali di tipo iperbolico o non locale ed applicazioni" and of University of Ferrara, FIR Project 2019 "Leggi di conservazione di tipo iperbolico: teoria ed applicazioni".

References

[1] Adimurthi, Dutta, R., Ghoshal, S. S., Veerappa Gowda, G. D., *Existence and nonexistence of TV bounds for scalar conservation laws with discontinuous flux*, Comm. Pure Appl. Math. **64** (1) (2011), 84–115.

[2] Adimurthi, Dutta, R., Gowda, G. D. V., Jaffré, J., *Monotone (A, B) entropy stable numerical scheme for scalar conservation laws with discontinuous flux*, ESAIM Math. Model. Numer. Anal. **48** (6) (2014), 1725–1755.

[3] Adimurthi, Mishra, S., Gowda, G. D. V., *Optimal entropy solutions for conservation laws with discontinuous flux-functions*, J. Hyperbolic Differ. Equ. **2** (4) (2005), 783–837.

[4] Adimurthi, Mishra, S., Gowda, G. D. V., *Existence and stability of entropy solutions for a conservation law with discontinuous non-convex fluxes*, Netw. Heterog. Media **2** (1) (2007), 127–157.

[5] Andreianov, B., *The semigroup approach to conservation laws with discontinuous flux*, in: *Hyperbolic conservation laws and related analysis with applications*, Springer Proc. Math. Stat. **49**, Springer, Heidelberg, 2014, 1–22.

[6] Andreianov, B., *New approaches to describing admissibility of solutions of scalar conservation laws with discontinuous flux*, in: *CANUM 2014 – 42e Congrès National d'Analyse Numérique*, ESAIM Proc. Surveys **50** EDP Sci., Les Ulis, 2015, 40–65.

[7] Andreianov, B., Cancès, C., *Vanishing capillarity solutions of Buckley–Leverett equation with gravity in two-rocks' medium*, Comput. Geosci. **17** (3) (2013), 551–572.

[8] Andreianov, B., Cancès, C., *On interface transmission conditions for conservation laws with discontinuous flux of general shape*, J. Hyperbolic Differ. Equ. **12** (2) (2015), 343–384.

[9] Andreianov, B., Donadello, C., Rosini, M. D., *A second-order model for vehicular traffics with local point constraints on the flow*, Math. Models Methods Appl. Sci. **26** (4) (2016), 751–802.

[10] Andreianov, B., Karlsen, K. H., Risebro, N. H., *A theory of L^1-dissipative solvers for scalar conservation laws with discontinuous flux*, Arch. Ration. Mech. Anal. **201** (1) (2011), 27–86.

[11] Andreianov, B., Mitrović, D., *Entropy conditions for scalar conservation laws with discontinuous flux revisited*, Ann. Inst. H. Poincaré Anal. Non Linéaire **32** (6) (2015), 1307–1335.
[12] Andreianov, B., Rosini, M. D., *Microscopic selection of solutions to scalar conservation laws with discontinuous flux in the context of vehicular traffic*, submitted, 2019.
[13] Aw, A., Rascle, M., *Resurrection of "second order" models of traffic flow*, SIAM J. Appl. Math. **60** (3) (2000), 916–938.
[14] Bürger, R., Karlsen, K., Risebro, N., Towers., J., *Monotone difference approximations for the simulation of clarifier-thickener units*, Computing and Visualization in Science **6** (2) (2004), 83–91.
[15] Bürger, R., Karlsen, K. H., Towers, J. D., *An Engquist–Osher-type scheme for conservation laws with discontinuous flux adapted to flux connections*, SIAM J. Numer. Anal. **47** (3) (2009), 1684–1712.
[16] Bürger, R., Karlsen, K. H., Towers, J. D., *On some difference schemes and entropy conditions for a class of multi-species kinematic flow models with discontinuous flux*, Netw. Heterog. Media **5** (3) (2010), 461–485.
[17] Cancès, C., *Asymptotic behavior of two-phase flows in heterogeneous porous media for capillarity depending only on space. I. Convergence to the optimal entropy solution.* SIAM J. Math. Anal. **42** (2) (2010), 946–971.
[18] Colombo, R. M., Goatin, P., *A well posed conservation law with a variable unilateral constraint*, J. Differential Equations **234** (2) (2007), 654–675.
[19] Di Francesco, M., Fagioli, S., Rosini, M. D., *Many particle approximation of the Aw–Rascle–Zhang second order model for vehicular traffic*, Math. Biosci. Eng. **14** (1) (2017), 127–141.
[20] Diehl, S., *Continuous sedimentation of multi-component particles*, Math. Methods Appl. Sci. **20** (15) (1997), 1345–1364.
[21] Diehl, S., *A uniqueness condition for nonlinear convection-diffusion equations with discontinuous coefficients*, J. Hyperbolic Differ. Equ. **6** (1) (2009), 127–159.
[22] Garavello, M., Natalini, R., Piccoli, B., Terracina, A., *Conservation laws with discontinuous flux*, Netw. Heterog. Media **2** (1) (2007), 159–179.
[23] Ghoshal, S. S., *Optimal results on TV bounds for scalar conservation laws with discontinuous flux*, J. Differential Equations **258** (3) (2015), 980–1014.
[24] Gimse, T., Risebro, N. H., *Solution of the Cauchy problem for a conservation law with a discontinuous flux function*, SIAM J. Math. Anal. **23** (3) (1992), 635–648.
[25] Hopf, E., *The partial differential equation* $u_t + uu_x = \mu u_{xx}$, Comm. Pure Appl. Math. **3** (1950), 201–230.
[26] Kaasschieter, E. F., *Solving the Buckley–Leverett equation with gravity in a heterogeneous porous medium*, Comput. Geosci. **3** (1) (1999), 23–48.
[27] Karlsen, K. H., Risebro, N. H., Towers, J. D., L^1 *stability for entropy solutions of nonlinear degenerate parabolic convection-diffusion equations with discontinuous coefficients*, Skr. K. Nor. Vidensk. Selsk. **3** (2003), 49 pp.
[28] Kruzhkov, S. N., *First order quasilinear equations with several independent variables*, Mat. Sb. (N. S.) **81** (123) (1970), 228–255.
[29] Lighthill, M., Whitham, G., *On kinematic waves II. A theory of traffic flow on long crowded roads*, Proc. R. Soc. Lond. Ser. A Math. Phys. Eng. Sci. **229** (1955), 317–345.
[30] Rayleigh, L., *Aerial plane waves of finite amplitude* [Proc. R. Soc. Lond. Ser. A Math. Phys. Eng. Sci. **84** (1910), 247–284], in: *Classic Papers in Shock Compression Science*, High-press, Shock Compression Condens. Matter, Springer, New York, 1998, 361–404.
[31] Richards, P. I., *Shock waves on the highway*, Operations Research **4** (1) (1956), 42–51.

[32] Seguin, N., Vovelle, J., *Analysis and approximation of a scalar conservation law with a flux function with discontinuous coefficients*, Math. Models Methods Appl. Sci. **13** (2) (2003), 221–257.
[33] Shen, W., *Traveling wave profiles for a follow-the-leader model for traffic flow with rough road condition*, Netw. Heterog. Media **13** (3) (2018), 449–478.
[34] Shen, W., *Traveling waves for conservation laws with nonlocal flux for traffic flow on rough roads*, Netw. Heterog. Media **14** (4) (2019), 709–732.
[35] Towers, J. D., *Convergence of a difference scheme for conservation laws with a discontinuous flux*, SIAM J. Numer. Anal. **38** (2) (2000), 681–698.
[36] Zhang, H., *A non-equilibrium traffic model devoid of gas-like behavior*, Transportation Research Part B: Methodological **36** (3) (2002), 275–290.

M. D. Rosini
Institute of Mathematics
Maria Curie-Skłodowska University
pl. Marii Curie-Skłodowskiej 1, 20-031 Lublin
Poland
e-mail: massimiliano.rosini@poczta.umcs.lublin.pl

Department of Mathematics and Computer Science
University of Ferrara, I-44121
Italy

Received July 25, 2019